ELECTROSTATICS OF POLYMER TRANSLOCATION THROUGH MEMBRANE NANOPORES IN ELECTROLYTE SOLUTIONS

A THESIS SUBMITTED TO

THE GRADUATE SCHOOL OF ENGINEERING AND SCIENCE

OF BILKENT UNIVERSITY

IN PARTIAL FULFILLMENT OF THE REQUIREMENTS FOR

THE DEGREE OF

MASTER OF SCIENCE

IN

PHYSICS

By

Ghada Mahmoud Abdullah Mohamed

February 2021

Electrostatics of Polymer Translocation through Membrane Nanopores
in Electrolyte Solutions
By Ghada Mahmoud Abdullah Mohamed
February 2021

We certify that we have read this thesis and that in our opinion it is fully adequate, in scope and in quality, as a thesis for the degree of Master of Science.

Şahin Büyükdağlı(Advisor)

Mehmet Cemal Yalabık

Mehmet Emre Taşgın

Approved for the Graduate School of Engineering and Science:

Ezhan Karaşan
Director of the Graduate School

ABSTRACT

ELECTROSTATICS OF POLYMER TRANSLOCATION THROUGH MEMBRANE NANOPORES IN ELECTROLYTE SOLUTIONS

Ghada Mahmoud Abdullah Mohamed
M.S. in Physics
Advisor: Şahin Büyükdağlı
February 2021

The transport of polymers across membranes in electrolyte solutions happens in most biological systems and is necessary for cells to function. Moreover, the polymer translocation process has proven to be very important in experiments and applications as well, providing a rich source of information about the polymer's size and composition [1], [2], making the polymer translocation procedure a potential sequencing method that is efficient, cheap, and quick [3], [4]. However, no consensus on the theoretical understanding of the translocation mechanism has been reached yet [3], leaving it a major challenge for theoretical modelling due to its steric, hydrodynamic, and electrostatic interactions [2], [5]. Here, we calculate the electrostatic energy cost of the translocating polymer in both the approach and translocation phases and investigate the dependence of the polymer's grand potential on different model tunable parameters. In the case of neutral membranes, low permittivity carbon-based membranes repel the approaching polymer with energy magnitude between $\sim 11\ k_{\mathrm{B}}T$ and $\sim 27\ k_{\mathrm{B}}T$, while high permittivity engineered membranes attract the approaching polymer with almost the same energy magnitude. This behavior can be attributed to polymer image-charge interactions, which become amplified with low permittivity membranes. In strong salt solutions, the membrane exhibits a repulsive barrier that turns to a metastable well in dilute solutions. In pure solvents, the metastable well becomes a deep, stable well that traps the polymer in the pore for some time, where the translocation phase is mainly governed by the attractive trans-cis side interaction. For weakly charged membranes, the membrane charge attraction wins over the image-charge repulsion, leading to an attractive minimum at $z_t \approx -1$ nm followed by a repulsive barrier at $l_t = L/2$ while for stronger membrane charges, the attractive well turns to a metastable point followed by an attractive, stable well. These results suggest that, in translocation experiments, DNA motion can

be controlled by tuning the system parameters, such as the solution concentration or the membrane charge.

Keywords: Chemical Physics, Soft-matter, Biophysics, Polymer Physics, Polymer Translocation, DNA sequencing, Gene therapy.

ÖZET

ELEKTROLIT IÇEREN NANOPORLARDAN POLIMER TRANSLOKASYONUNUN ELEKTROSTATIĞI

Ghada Mahmoud Abdullah Mohamed
Fizik, Yüksek Lisans
Tez Danışmanı: Şahin Büyükdağlı
Şubat 2021

DNA gibi yüklü polimerlerin genetik kodunun polimer translokasyonu yöntemiyle okunabilmesi için, DNA'nın yüksek süratle nanopora çekilip, translokasyon süresinin uzatılması amacıyla nanoporda yavaşlatılması gerekir. Bu şartları sağlayan deneysel koşulları belirlemek için, elektrolit rezervuarına bağlı nanoporlardan yüklü polimerlerin geçişi için gerekli elektrostatik enerjiyi hesaplıyoruz. Bu amaçla, polymer ve yüzeyi yüklü nanoporla etkileşen Coulomb sıvısının istatistiksel dağılım fonksiyonunu fonksiyonel integral yaklaşımıyla ifade ediyoruz. Bu fonksiyonel integrali yaklaşık yöntemlerle hesaplayarak polimerin serbest enerjisini çıkarıyoruz. Serbest enerjinin ion yoğunluğu ve nanopor yüzey yükü gibi deneysel olarak kontrol edilebilen parametrelerle değişimini inceleyerek optimal translokasyon şartlarını belirliyoruz.

Anahtar sözcükler: Kimyasal fizik, yumuşak madde fiziği, biofizik, polimer fiziği, polimer translokasyonu, DNA dizileme, gen terapisi.

Acknowledgement

I would like to express my sincere gratitude for my friends Noor Yousuf, Mustafa Amin, and Amr Mamdouh for their help with some Maths tricks and technical bugs, and Ahmed Ouf -a Bilkent Physics alumnus- for his continuous support that began even before I came to Bilkent ...

Contents

List of Figures

List of Tables

Chapter 1

Introduction

Assume you have got a hole in the glass of your room window on a windy day. Wind will keep entering the room through that hole, making a rather noisy sound. You will probably try to think of a handy solution using anything you already have in the room, say, a piece of cloth or a crumpled up plastic bag, and stuff it in the hole. Clearly, according to how well the piece of cloth fits in the hole, more or less wind will seep into the room.

This basic idea of common sense seems to happen in many biological systems and is even used in experimental set-ups. Replace the glass window with a double-layered lipid membrane, with a hole in it in the form of an embedded protein channel or pump, and you have got yourself an ion channel, or a membrane pore that happens to exist abundantly in the cells of most of the biological systems. Apply a voltage difference across that membrane, and you will have a current going through the channel, consisting of the ions present on both sides of the membrane (the wind in the case of the window). Now, plug a polymer (the piece of cloth) in that channel, like a protein or an mRNA, you will notice that the ionic current will drop drastically since the ions will not be able to move, but once the polymer slips through to the other side, the ionic current will return to its previous value.

On a larger scale, ion channels and membrane pores exist in biological systems in all shapes and sizes and carry out different functions. Ion channels are water-filled

holes that allow for the exchange of ions between both sides of the cell membrane. Their pores are mainly protein pumps embedded in the phospholipid membrane, which can be either open or closed, and when open, they are specific to the type of ions they allow to pass [6]. Ion channels can be ligand-gated [1], mechanically-gated [2], or voltage-gated [3] that use either passive transport [4] like Sodium-ion or Potassium-ion channels or active transport [5] like the Sodium-Potassium pump. There is also the nuclear pore complex, which spans the double-layered nucleus membrane and allows for polymers like polymerase and mRNA into and out of the nucleus, respectively. Examples of other ion channels include mitochondrial channels and protein-conducting channels in the endoplasmic reticulum [2].
This transport of proteins or poly-nucleotides through membrane pores is involved in many processes such as DNA and RNA transport across the nuclear membrane and protein transport through cellular membrane [7], phage infection [8], and injection of viral DNA [7].
Generally speaking, most cells need to transport macromolecules across membranes to function, and in some cases, quite thick molecules can pass through nanoscale channels [8].

Application-wise, this principle has been around in experiments for quite some time. The first attempt was the Coulter counter, developed by Wallace Coulter in the 1940ies and later patented in 1953 [9]. Coulter's approach was based on the measurement of the change in impedance proportional to the size of an object passing through an orifice displacing some of the electrolyte and carrying along the current in an electric field [3]. It has been since used in counting blood cells, but it was shown later that it could also be used to count sub-micron objects like viruses [10].
However, this field has started to flourish and be flooded with research papers,

[1] Ligand-gated ion channels open when a specific neurotransmitter or a hormone holds onto its protein pump.
[2] Mechanically-gated ion channels open in response to the physical stretching of the cell membrane.
[3] Voltage-gated ion channels open under the influence of chemical gradient across the cell membrane.
[4] Ion diffusion or movement under an ion concentration gradient.
[5] Ion movement against the concentration gradient.

experiments, simulations, and theoretical models since the landmark papers by Bezrukov in 1994 and that by Kasianowicz in 1996. In 1994, Bezrukov *et al.* demonstrated that poly(ethylene oxide) molecules could be counted from the time trace of the ionic current passing through an alamethicin channel [11]. Two years later, Kasianowicz *et al.* showed that an electric field generated by a trans-membrane voltage and applied across a continuously open 2.6-nm diameter α-hemolysin ion channel suspended in a lipid bilayer membrane could drive a single-stranded DNA and RNA through that channel in a process called "translocation". They found that during the passage of the DNA as an extended chain, the ionic current is partially or mostly blocked, and that the passage of each molecule corresponds to a reduction in the ionic current signal, whose duration is proportional to the polymer length. They reasoned that these current signal blockades could be used to measure the poly-nucleotide length and possibly other characteristics [1]. Later on, it was argued that the current blockades were not only sensitive to the polymer length, but also to the polymer composition, secondary structure, and to even other physical parameters of the system like the temperature, ionic strength, and driving field intensity, which makes these blockades a rich source of information about the dynamics of polymers in membrane pores [2].

In their paper, Kasianowicz *et al.* argued that proteins could also pass through lipid bilayers through protein translocating channels, again as unfolded, extended chains. They also stated that with further improvements, their translocation method could be used as a fast and direct technique to detect the sequence of nucleotides in single DNA or RNA molecules [1]. Since then, their method has been used to characterize objects like single or double-stranded DNA and RNA, proteins, and cells, and to analyze their properties [7], and scientists have been working on how to implement and optimize this method to decipher the sequence of nucleotide bases in DNA. Some scientists even speculated that it could be used in medical diagnostics [4] and gene therapy [8]. This translocation phenomenon's significant potential as a sequencing method is that it would be efficient, cheap, and quick [3], [4].

Although, in the recent decades after Kasianowicz's paper, dozens of research studies have been conducted on the translocation phenomenon, visioning its use

as a sequencing method, this goal has not been achieved yet [3]. This can be attributed to our limited understanding of the polymer translocation mechanism, especially when the external electric field is weak, and the translocation process is mainly governed by entropic barriers [7].
In the light of papers in the literature that attempted to understand the polymer translocation process statistically, polymer translocation can be divided into two categories: forced translocation, which can be under the effect of chemical interaction [3], [7], or electrophoresis [6] [8], [7] , [4], and unforced translocation, which is governed mainly by the polymer free energy and other entropic parameters.

In literature, most of the conducted experiments used the external electric field as a driving force, with few others that used methods like chaperone binding and polymer adsorption [3]. Due to this intensive studying, forced translocation is so far pretty understood, which creates a discrepancy between our theoretical understanding of the forced and unforced translocation and leaves unforced translocation a major challenge for theoretical modeling [3]. Another reason for the great interest in the translocation process -and a reason for its complexity- lies in studying the steric [7], electrostatic, and hydrodynamic interactions between the polymer and the solvent molecules, the ions, the membrane, and the pore confining walls [2], [5]. In the literature of theoretical modelling of unforced translocation, the translocation process is implicitly divided into two phases: first, the "capture" or "approach" phase in which the polymer is threaded at a small distance on the CIS side of the membrane, and second, the "translocation" phase in which the polymer slides through the pore into the TRANS side of the membrane.
The first approach to model the translocation process was introduced in the leading article of Sung and Park in 1996 [13], in which they managed to write the polymer free energy, which happened to create an entropic barrier that must be overcome for a successful translocation event. They also found that in the limit of

[6] Electrophoresis is the migration of poly-electrolyte chains driven by external electric field [12].
[7] Relating to the atoms' spatial arrangement.

very long polymers, this entropic barrier becomes so large that it would be practically almost impossible to overcome in an unforced translocation [13]. Polymer length happens to be a crucial parameter in the translocation process. In 1999, Lubensky *et al.* [8] showed a range of polymer lengths for which the system can almost preserve its translational invariance. They also designed a microscopic model in which the polymer's speed depends on its chemical composition and even its orientation in the channel. Since the paper of Sung and Park, many studies have considered the different parameters and scenarios for the various interactions in the translocation process. Some of them considered, for example, the confinement of polymers in channels with diameters significantly larger than polymers' length, while others considered the opposite limit of very narrow pores [8].

The theoretical study reproduced in this thesis is a tiny step in quantitatively assessing the electrostatic interaction between the translocating polymer and its surrounding medium in an unforced translocation event. The main goal consists in calculating the electrostatic energy cost or the electrostatic contribution to the energy barrier in both the approach and the translocation phases in the polymer translocation event, and evaluating the behavior of the electrostatic potential based on different parameters in the system, trying to reach the optimum values for each parameter that minimize the energy barrier. This is done by following the steps of Büyükdağlı and Ala-Nissila in their two 2016 articles [14], [5], recovering their model and reproducing some of their results. One of the limitations of formalisms previous to these two papers, like the one in 2014 by the same authors [15] is that they account exclusively for the DNA portions inside the membrane pore. This could be valid in the case of thick membranes like the one in the numerical study by Levitt *et al.* in 1978 where they considered a channel of length $d = 25$ Å [16]. However, for the current graphene-based membranes used in translocation experiments, which have thickness reduced to $d = 6$ Å, at any given time during the experiment, most of the polymer's segments will be either on the CIS or the TRANS side subject to image-charge forces induced by the dielectric mismatch between the membrane and the solvent, whose influence on

the translocation process cannot be ignored. Therefore, a polymer translocation model considering the polymer segments outside the pore is presented, including the image-charge interactions.

Chapter 2 lays the foundation for describing the electric potential's behavior in a solution where the charges follow the Boltzmann distribution. This is done by deriving the Poisson-Boltzmann (PB) equation in the light of the electric double layer model.
In Chapter 3, PB Eq. is solved analytically in the case of planar and cylindrical geometries.
In Chapter 4, we aim at describing a charged liquid mathematically by deriving the functional integral form of the partition function, then we move on to deduce the electrostatic grand potential of the system at the Debye-Hückel (DH) level.
In Chapter 5, which has most of the work and the results, we formulate the electrostatic translocation model of a polymer translocating through a membrane in a charged liquid without an external force in both of the approach and translocation phases. After that, we test the effect of different parameters, i.e., the membrane permittivity, the bulk concentration, the polymer length, and the membrane charge density on the grand potential profile, to reach a consensus on their optimum values.

Chapter 2

Poisson-Boltzmann Formalism

Poisson-Boltzmann equation describes a model developed independently by Louis Georges Gouy [17] and David Leonard Chapman [18] in the past century. In this model, ions of a solution come into contact with a charged layer, where a layer of counterions from a weak electrolyte forms near the solid charged one, known as the electric double layer model. The mathematical formulation of the model was later developed by Debye and Hückel [19]. The Poisson-Boltzmann equation describes the electrostatic potential distribution at a charged surface in a direction normal to the charged layer. The Poisson-Boltzmann model uses the mean-field (MF) approximation [20], and neglects the finite size of the solution ions, considering them as point charges that interact with the average electric field of the neighbouring ions instead of each ion individually. It also assumes a homogeneous surface charge distribution on the charged layer. The equation is used in many fields and has different corresponding versions; it is used in material science, polymer science, and physiology to calculate the potential of charged macromolecules.

In this chapter, we explain the Poisson-Boltzmann formalism, describing the electric potential's behavior when the charges in a solution follow the Boltzmann distribution. For this goal, we first need to identify three parameters:

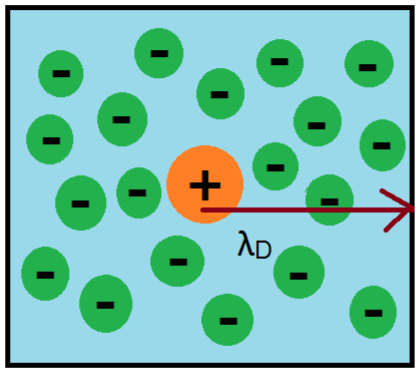

Figure 2.1: Debye-Hückel Screening Length is the radius of the ionic cloud.

1) Bjerrum Length l_B:

The Bjerrum length is defined as the inter-ionic separation distance at which the electrostatic energy equals the thermal energy k_BT. From this definition, the Bjerrum length follows as:

$$l_B = \frac{e^2}{4\pi\epsilon_w k_B T} \quad , \tag{2.1}$$

where e is the charge of the electron, ϵ_w is the permittivity of water, T is the temperature, and k_B is the Boltzmann constant.

2) Debye-Hückel Screening Length λ_D:

The Debye-Hückel length plays a key role in Plasma Physics and the electrostatics of charged liquids. It is defined as the radius of the counter-ion cloud around a central charge ion. It is defined as:

$$\lambda_D = (8\pi l_B n_0)^{-1/2} = \sqrt{\frac{\epsilon k_B T}{2 n_0 e^2}} \quad , \tag{2.2}$$

where n_0 is the bulk ion concentration.

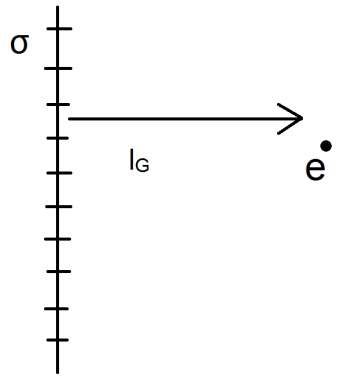

Figure 2.2: Gouy-Chapman Length.

For the remainder, we introduce the screening parameter κ corresponding to the inverse Debye-Hückel length,

$$\kappa = \lambda_D^{-1} = \sqrt{8\pi l_B n_0} = \sqrt{\frac{2n_0 e^2}{\epsilon k_B T}} \quad . \tag{2.3}$$

3) Gouy-Chapman Length l_G:

The Gouy-Chapman length is the equivalent of the Bjerrum length in the case of an ion and a surface, instead of two ions. Thus, it can be defined as the distance at which the electrostatic energy between an ion and a charged plane is equal to the thermal energy, or the distance at which an ion interacts with a charged membrane with an energy equal to $k_B T$, i.e.

$$l_G = \frac{2\epsilon k_B T}{e\sigma} \quad , \tag{2.4}$$

where $\sigma > 0$ is the magnitude of the negative membrane surface charge.

We now consider an ionic solution including both positive and negative ions. The salt concentration of the solution is $\rho = \rho_+ + \rho_-$. The charge density can be written as $\rho = nze$ or $\rho(\mathbf{r}) = n(\mathbf{r})ze$, where $n(\mathbf{r})$ is the number density of ions at the position $\mathbf{r}$, and z is the ion valency.
The electrostatic boundary conditions to be applied can be a constant potential

(Dirichlet B.C.) or a constant charge density (Neumann B.C.) of the membrane surface. At any point $\mathbf{r}$, the relation between ϕ (potential) and ρ can be described by Poisson's equation

$$\nabla^2\phi(\mathbf{r}) = -\frac{\rho(\mathbf{r})}{\epsilon} \quad , \tag{2.5}$$

or

$$\nabla^2\phi(\mathbf{r}) = -\frac{e}{\epsilon}\left[z_+ n_+(\mathbf{r}) + z_- n_-(\mathbf{r})\right] \quad , \tag{2.6}$$

where z_+ is the valency of the cations and z_- is the valency of the anions.
Since the ion species are in thermal equilibrium, their number densities obey the Boltzmann distribution

$$n_\pm(\mathbf{r}) = n_\pm^0 e^{-ez\phi(\mathbf{r})/k_BT} \quad , \tag{2.7}$$

where $n_\pm^0$ is the bulk ion concentration (note that $n_\pm(\mathbf{r}) \longrightarrow n_\pm^0$ as $\phi \longrightarrow 0$ in the bulk).
Now, we can write the general form of Poisson-Boltzmann equation as

$$\nabla^2\phi(\mathbf{r}) = -\frac{e}{\epsilon}\left[z_+ n_+^0 e^{-ez_+\phi(\mathbf{r})/k_BT} + z_- n_-^0 e^{-ez_-\phi(\mathbf{r})/k_BT}\right] \quad , \tag{2.8}$$

which can be recast as

$$\nabla^2\phi(\mathbf{r}) = -\frac{e}{\epsilon}\sum_{i=\pm} z_i n_i^0 e^{-ez_i\phi(\mathbf{r})/k_BT} \quad . \tag{2.9}$$

Another way to derive Eq.(2.7) consists in requiring that the chemical potential for both ion species would be constant, that is

$$\mu_\pm = ez_\pm\phi + k_BT\ln(n_\pm) = C \quad . \tag{2.10}$$

The exponential of Eq.(2.10) yields directly Eq.(2.7).
In the case of a solution containing only a single counter-ion species, i.e. for $n_- = 0$ and $n_0 = n_+$, Eq.(2.8) becomes

$$\nabla^2\phi(\mathbf{r}) = -\frac{e}{\epsilon}z_+ n_0 e^{-ez_+\phi(\mathbf{r})/k_BT} \quad . \tag{2.11}$$

We consider now the case of a monovalent ionic solution, such as NaCl. Setting $z_\pm = \pm 1$ and $n_+^0 = n_-^0 = n_0$, Eq.(2.8) becomes

$$\nabla^2\phi(\mathbf{r}) = -\frac{e}{\epsilon}\left[n_0 e^{-e\phi(\mathbf{r})/k_BT} - n_0 e^{e\phi(\mathbf{r})/k_BT}\right] \quad , \tag{2.12}$$

or

$$\nabla^2\phi(\mathbf{r}) = \frac{2en_0}{\epsilon}\sinh\left(\frac{e\phi(\mathbf{r})}{k_BT}\right) \quad . \tag{2.13}$$

In the DH regime $\kappa l_B >> 1$ where $\phi << 1$, Eq.(2.12) can be Taylor-expanded in terms of ϕ. This yields

$$\nabla^2\phi(\mathbf{r}) = \frac{2e^2n_0}{\epsilon k_BT}\phi(\mathbf{r}) \quad , \tag{2.14}$$

which can be recast as

$$\nabla^2\phi(\mathbf{r}) = \lambda_D^{-2}\phi(\mathbf{r}) = \kappa^2\phi(\mathbf{r}) \quad , \tag{2.15}$$

where λ_D is Debye-Hückel screening length, and κ is its inverse. The DH Eq. (2.15) will be solved in the next chapter in the cylindrical nanopore geometry.

Chapter 3

Solution of Poisson-Boltzmann Equation in Plane and Cylindrical Geometry

As the Poisson-Boltzmann equation is a second-order partial differential equation, it is usually solved numerically. However, in specific geometries possessing a symmetry, it can be solved analytically. In this chapter, we solve the Poisson-Boltzmann equation analytically in planar and cylindrical geometries.

3.1 Plane Geometry

Here, we carry out the non-linear Poisson-Boltzmann equation's analytical solution for the counter-ion-only liquid and a symmetric salt solution.

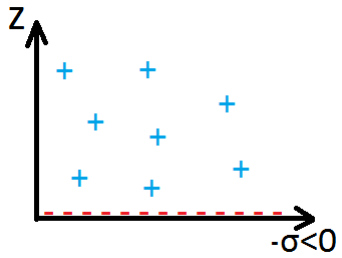

Figure 3.1: Schematic depiction of the counter-ion-only liquid in contact with a negatively charged membrane surface.

3.1.1 Counter-Ion only Case

Due to the interfacial charge configuration, this case is also called the electric double-layer problem, where one has fixed negative surface charges of density $-|\sigma| < 0$ acting as anions, and counter-ions in the solution corresponding to monovalent cations ($z_+ = 1$ and $n(z) = n_+(z)$). Eq. (2.11) then becomes

$$\nabla^2(\phi) = -\frac{e}{\epsilon} n_0 e^{-\frac{e\phi(z)}{k_B T}} \quad , \tag{3.1}$$

with the boundary condition following from Gauss' law

$$\left.\frac{d\phi}{dz}\right|_{z=0} = \frac{\sigma}{\epsilon} \quad . \tag{3.2}$$

By multiplying both sides of Eq.(3.1) with $\frac{d\phi}{dz}$, and carrying out integration by parts, one gets

$$\left(\frac{d\phi}{dz}\right)^2 = \frac{2k_B T}{\epsilon} e^{-\frac{e\phi(\mathbf{r})}{k_B T}} - C \quad , \tag{3.3}$$

where C is an integration constant.

To find C, we consider the bulk limit $z \to \infty$ of Eq.(3.3) where the field and the potential vanish. This yields

$$\left(\frac{d\phi}{dz}\right)^2 = \frac{2k_B T}{\epsilon} \left(e^{-\frac{e\phi(\mathbf{r})}{k_B T}} - 1\right) \quad . \tag{3.4}$$

Integrating Eq.(3.4) via two successive substitutions, the potential follows as

$$\phi(z) = \frac{2k_B T}{e} \ln\left(z + \frac{\epsilon_D k_B T}{2\pi e \sigma_0}\right) + \phi_0 \quad , \tag{3.5}$$

where ϵ_D is the dielectric constant of water and ϕ_0 is an arbitrary reference potential.

3.1.2 Added Electrolyte Case

Consider a negatively charged surface at $z = 0$ in contact with an electrolyte bath, with the boundary condition in Eq.(3.2) of the previous case. The electrolyte is monovalent, i.e. $z_\pm = 1$. In addition, in the bulk region at $z = \infty$, one has $\phi(\infty) = 0$ and $n(\infty) = n_0$, where n_0 is the bulk salt concentration.
Recall now from the previous chapter the form of the Poisson-Boltamzann equation for a symmetric salt solution,

$$\nabla^2\phi(z) = \frac{2en_0}{\epsilon}\sinh\left(\frac{e\phi(\mathbf{r})}{k_BT}\right) \quad . \tag{3.6}$$

Multiplying both sides with $\frac{d\phi}{dz}$, and carrying out an integration by parts, we get

$$\left(\frac{d\phi}{dz}\right)^2 = \frac{4n_0k_BT}{\epsilon}\cosh\left(\frac{e\phi(z)}{k_BT}\right) + C \quad , \tag{3.7}$$

where C is a constant of integration. Taking the bulk limit where $\phi \to 0$ and $\phi' \to 0$, one gets $C = \frac{-4n_0k_BT}{\epsilon}$. Eq.(3.7) becomes

$$\left(\frac{d\phi}{dz}\right)^2 = \frac{4n_0k_BT}{\epsilon}\left(\cosh\left(\frac{e\phi(z)}{k_BT}\right) - 1\right) \quad . \tag{3.8}$$

Taking now the square root of Eq.(3.8), separating the variables z and ϕ on different sides of the equation, and using trignometric identities, one obtains

$$\frac{d\phi}{\sinh\left(\frac{e\phi}{4k_BT}\right)\cosh\left(\frac{e\phi}{4k_BT}\right)} = \pm 4\sqrt{\frac{2n_0k_BT}{\epsilon}}dz \quad , \tag{3.9}$$

which can be recast as

$$d\ln\left(\tanh\left(\frac{e\phi}{4k_BT}\right)\right) = \frac{e}{4k_BT}\frac{d\phi}{\sinh\left(\frac{e\phi}{4k_BT}\right)\cosh\left(\frac{e\phi}{4k_BT}\right)} \quad . \tag{3.10}$$

Integrating Eq.(3.10), one gets

$$\ln\left(\tanh\left(\frac{e\phi}{4k_BT}\right)\right) = \pm\kappa(z - z_0) \quad , \tag{3.11}$$

where κ is the inverse of the DH screening length. The vanishing potential in the bulk $z \to \infty$ implies that one should keep the solution with the minus sign.

Then, in order to simplify the notation, we introduce the parameter $\gamma = e^{\kappa z_0}$. Finally, using the equality

$$\tanh\left(\frac{\phi}{2}\right) = \frac{e^{\phi/2}-1}{e^{\phi/2}+1} \quad , \tag{3.12}$$

and rearranging the equation, the potential function follows as

$$\phi(z) = \frac{-2k_BT}{e}\ln\left(\frac{1+\gamma e^{-\kappa z}}{1-\gamma e^{-\kappa z}}\right) \quad . \tag{3.13}$$

Now, we need to find the integration constant z_0, or equivalently, γ. To this aim, we impose the boundary condition (3.2) to Eq.(3.13). One obtains

$$\gamma = \frac{-2\kappa l_G \pm \sqrt{4\kappa^2 l_G^2 + 4}}{2} \quad . \tag{3.14}$$

To determine the sign, we recall that γ is an exponential function that can be only positive. One thus gets

$$\gamma = -\kappa l_G + \sqrt{\kappa^2 l_G^2 + 1} \quad . \tag{3.15}$$

Plugging now Eq.(3.13) into Eq.(2.7) and keeping in mind that $z_\pm = \pm 1$, the ion density follows as

$$n_\pm(z) = n_\pm^0 \ln\left(\frac{1\pm\gamma e^{-\kappa z}}{1\mp\gamma e^{-\kappa z}}\right)^2 \tag{3.16}$$

3.2 Cylindrical Geometry

Here, the Poisson-Boltzmann Equation is solved in cylindrical geometry to model the accumulation of charges around a rod-like charged object, such as a DNA molecule translocating through a nanopore.

Cell Model: The system is composed of two concentric cylinders confining an ionic solution in between them. The inner cylinder models a charged and elongated particle, while the outer one corresponds to a nanopore. Due to the cylindrical symmetry, the potential varies only in the radial direction. The inner cylinder of radius a has negative charge density ($-|\sigma| < 0$). Thus, one can define

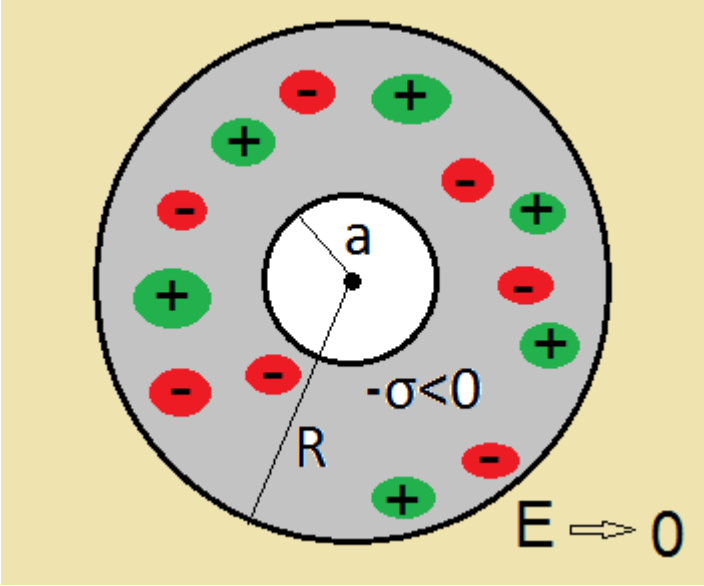

Figure 3.2: Accumulation of charges around a rod-like object of radius a and surface charge density $-|\sigma| < 0$ confined to a pore of radius R.

the line charge density of the polymer as $\lambda = 2\pi a|\sigma/e|$. As the surface of the pore carries no charge, the field vanishes at its interface. Thus, the boundary conditions read

$$\frac{d\phi}{ds}|_{s=a} = \frac{\sigma}{\epsilon} = \frac{e}{2\pi\epsilon}\frac{\lambda}{a} \quad , \tag{3.17}$$

$$\frac{d\phi}{ds}|_{s=R} = 0 \quad . \tag{3.18}$$

Here, we solve the linearized Poisson-Boltzmann equation in the added electrolyte case. Recalling Eq.(2.15), with the Laplacian operator in the cylindrical coordinates, and assuming an infinitely long cylinder, the linear PB equation becomes

$$\frac{1}{s}\frac{\partial}{\partial s}\left(s\frac{\partial\phi}{\partial s}\right) = \kappa^2\phi(s) \quad , \tag{3.19}$$

or

$$\frac{\partial^2\phi}{\partial s^2} + \frac{1}{s}\frac{\partial\phi}{\partial s} - \kappa^2\phi = 0 \quad . \tag{3.20}$$

One notes that Eq.(3.20) has the form of the modified Helmholtz equation, whose solution is a combination of the modified Bessel functions of the first ($I_n(\kappa s)$) and second kind ($K_n(\kappa s)$) of the n^{th} order, i.e.

$$\phi(s) = AI_n(\kappa s) + Bk_n(\kappa s) \quad . \tag{3.21}$$

To find the constants A and B, we apply the boundary condition, in Eq.(3.19) and (3.20), knowing that

$$C_{\alpha-1}(x) + C_{\alpha+1}(x) = 2\frac{dC_\alpha}{dx} \quad , \tag{3.22}$$

where C_α is either I_α or $e^{\alpha i\pi}K_\alpha$. In addition, due to azimuthal symmetry, we can set $n = 0$ in the modified Bessel functions. Performing these calculations, the potential follows as

$$\phi(s) = \frac{\sigma}{\epsilon\kappa}\frac{k_0(\kappa s)I_1(\kappa R) + I_0(\kappa s)K_1(\kappa R)}{K_1(\kappa R)I_1(\kappa a) - I_1(\kappa R)K_1(\kappa a)} \quad , \tag{3.23}$$

or

$$\frac{e\phi}{k_BT} = -\frac{2}{l_G\kappa}\frac{K_0(\kappa s)I_1(\kappa R) + I_0(\kappa s)K_1(\kappa R)}{K_1(\kappa a)I_1(\kappa R) - I_1(\kappa a)K_1(\kappa R)} \quad . \tag{3.24}$$

We explore now the asymptotic behaviour of this solution. Noting that in the limit $R \longrightarrow \infty$, one has $I_1(R) \longrightarrow \infty$, and $K_1(R) \longrightarrow 0$. Eq.(3.24) becomes

$$\frac{e\phi}{k_BT} = -\frac{2}{l_G\kappa}\frac{K_0(\kappa s)}{K_1(\kappa a)} \quad . \tag{3.25}$$

Furthermore, for $\kappa s >> 1$, or $s \longrightarrow \infty$, the function $K_0(\kappa s)$ behaves as

$$K_0(\kappa s) \approx \sqrt{\frac{\pi}{2s}}e^{-\kappa s}\left(1 + \frac{-1}{8\kappa s} + ...\right) \quad . \tag{3.26}$$

This finally yields the asymptotic large distance behaviour of the potential as

$$\phi \approx \frac{1}{\sqrt{s}}e^{-\kappa s} \quad . \tag{3.27}$$

Chapter 4

Functional Integral Formulation of the Coulomb Liquid Model

Here, we introduce the field-theoretic formulation of charged liquids. Our goal consists in deriving the functional integral form of the canonical partition function. The solution consists of p mobile ion species, each species i having N_i ions. The liquid also contains an arbitrary number of fixed charged sources, such as a DNA molecule, a membrane, or a protein.

4.1 Canonical Partition Function

The canonical partition function of the charged liquid reads

$$Z_c = \prod_{i=1}^{p} \prod_{j=1}^{N_i} \int d\mathbf{r}_{ij} e^{-\beta U} \quad , \tag{4.1}$$

where U stands for the total electrostatic interaction energy, and $\mathbf{r}_{ij}$ is the position vector of the ion j from the species i.
The total charge density of the system is

$$\rho(\mathbf{r}) = \sum_{i=1}^{p} \sum_{j=1}^{N_i} q_i \delta(\mathbf{r} - \mathbf{r}_{ij}) + \rho_0(\mathbf{r}) \quad , \tag{4.2}$$

where $\rho_0(\mathbf{r})$ is the fixed macromolecular charge density function.
The total potential energy of the system rescaled with the thermal energy $\beta^{-1} = k_B T$ can be expressed as

$$\beta U = \frac{1}{2} \int \int d\mathbf{r}^3 d\mathbf{r}'^3 \rho(\mathbf{r}) v_c(\mathbf{r}, \mathbf{r}') \rho(\mathbf{r}') + \sum_{i=1}^{p} \sum_{j=1}^{N_i} W_i(\mathbf{r}_{ij}) \quad . \tag{4.3}$$

In Eq.(4.3), the first term on the right hand side is the electrostatic interaction potential, and the second term is an on-site potential acting on the ion j of the species i.
The Coulomb potential is defined in terms of its inverse as

$$v_c^{-1}(\mathbf{r}, \mathbf{r}') = -\frac{k_B T}{e^2} \nabla_{\mathbf{r}} \epsilon(\mathbf{r}) \cdot \nabla_{\mathbf{r}'} \delta(\mathbf{r} - \mathbf{r}') \quad . \tag{4.4}$$

The Coulomb potential and its inverse are related by the convolution relation

$$\int d\mathbf{r}'' v_c^{-1}(\mathbf{r}, \mathbf{r}'') v_c(\mathbf{r}'', \mathbf{r}') = \delta(\mathbf{r} - \mathbf{r}') \quad . \tag{4.5}$$

Indeed, substituting Eq.(4.4) into Eq.(4.5), one obtains the differential equation solved by the Coulomb potential,

$$\nabla_{\mathbf{r}} \epsilon(\mathbf{r}) \cdot \nabla_{\mathbf{r}} v_c(\mathbf{r}, \mathbf{r}') = -\frac{e^2}{k_B T} \delta(\mathbf{r} - \mathbf{r}') \quad . \tag{4.6}$$

In Appendix B, we show that in a bulk system, the solution of Eq.(4.6) is the standard Coulomb potential

$$v_c(\mathbf{r} - \mathbf{r}') = \frac{l_B}{|\mathbf{r} - \mathbf{r}'|} \quad . \tag{4.7}$$

At this point, in order to recast the partition function (4.1) in an analytically manageable form, we switch from the electrostatic pairwise interaction picture to the picture of a single charge coupled to a background potential $\phi(\mathbf{r})$. This goal can be achieved by performing the following Hubbard Stratonovich transformation (see Appendix A for its derivation)

$$\begin{aligned} e^{-\beta U_{el}} &= e^{-\frac{\beta}{2} \int d\mathbf{r} d\mathbf{r}' \rho(\mathbf{r}) v_c(\mathbf{r}, \mathbf{r}') \rho(\mathbf{r}')} \\ &= \left[\det \left[\frac{v_c(\mathbf{r}, \mathbf{r}')}{\beta} \right] \right]^{-1/2} \int D\phi e^{-\frac{\beta}{2} \int d\mathbf{r} d\mathbf{r}' \phi(\mathbf{r}) v_c^{-1}(\mathbf{r} - \mathbf{r}') \phi(\mathbf{r}') + i\beta \int d\mathbf{r} \rho(\mathbf{r}) \phi(\mathbf{r})} \end{aligned} \quad , \tag{4.8}$$

where $\phi(\mathbf{r})$ is a background fluctuating potential dressed by the pairwise many-body interactions. From now on, we shall omit the determinant and the β factors for simplicity. Within the corresponding notations, the Boltzmann distribution reads

$$e^{-U_{el}} = \int D\phi e^{-\frac{1}{2}\frac{k_B T}{e^2}\int d\mathbf{r}\epsilon(\mathbf{r})[\nabla_r\phi(\mathbf{r})]^2 + i\int d\mathbf{r}\rho(\mathbf{r})\phi(\mathbf{r})} \quad . \tag{4.9}$$

Substituting Eq.(4.9) into Eq.(4.1), after some algebra, the canonical partition function becomes

$$\begin{aligned} Z_c = \int D\phi e^{-\frac{k_B T}{2e^2}\int d\mathbf{r}\epsilon(\mathbf{r})[\nabla_r\phi(\mathbf{r})]^2 + i\int d\mathbf{r}\rho_0(\mathbf{r})\phi(\mathbf{r})} \\ \times \prod_{i=1}^{p}\left[\int d\mathbf{r} e^{-W_i(\mathbf{r}) + iq_i\phi(\mathbf{r})}\right]^{N_i} \quad . \end{aligned} \tag{4.10}$$

One notes that in Eq.(4.10), the bracket term in front of the product sign corresponds to the partition function of a single charge experiencing the effective potential $U(\mathbf{r}) = -iq_i\phi(\mathbf{r}) + W_i(\mathbf{r})$.

4.2 Grand Canonical Partition Function

In order to account for the ion exchange between the interfacial and bulk regions, we now impose the chemical equilibrium between these zones. To this aim we pass from the canonical to the grand canonical ensemble.

The grand canonical partition function is related to the canonical one by the relation

$$Z_G = \prod_{i=1}^{p}\sum_{N_i}^{\infty}\frac{\lambda_i^{N_i}}{N_i!}Z_c \quad , \tag{4.11}$$

where λ_i is the ion fugacity. Plugging Eq.(4.10) into Eq.(4.11), one obtains

$$\begin{aligned} Z_G = \int D\phi e^{-\frac{k_B T}{2e^2}\int d\mathbf{r}\epsilon(\mathbf{r})[\nabla_r\phi(\mathbf{r})]^2 + i\int d\mathbf{r}\rho_0(\mathbf{r})\phi(\mathbf{r})} \\ \times \prod_{i=1}^{p}\sum_{N_i=1}^{\infty}\frac{1}{N_i!}\left[\lambda_i\int d\mathbf{r} e^{-W_i(\mathbf{r}) + iq_i\phi(\mathbf{r})}\right]^{N_i} \quad . \end{aligned} \tag{4.12}$$

Noting that the sum in Eq.(4.12) is the Taylor series of the exponential function, the grand canonical partition function takes the form

$$Z_G = \int D\phi e^{-\frac{k_B T}{2e^2}\int d\mathbf{r}\epsilon(\mathbf{r})[\nabla_r\phi(\mathbf{r})]^2 + i\int d\mathbf{r}\rho_0(\mathbf{r})\phi(\mathbf{r})} \times e^{\sum_{i=1}^{p}\lambda_i d\mathbf{r} e^{-W_i(\mathbf{r})+iq_i\phi(\mathbf{r})}} \quad . \tag{4.13}$$

Defining now the functional Hamiltonian of the system,

$$H[\phi(\mathbf{r})] = \frac{k_B T}{2e^2}\int d\mathbf{r}\epsilon(\mathbf{r})\left[\nabla_r\phi(\mathbf{r})\right]^2 - i\int d\mathbf{r}\rho_0(\mathbf{r})\phi(\mathbf{r}) - \sum_{i=1}^{p}\lambda_i\int d\mathbf{r} e^{-W_i(\mathbf{r})+iq_i\phi(\mathbf{r})} \quad , \tag{4.14}$$

the grand canonical partition function can be recast as a functional integral, i.e.

$$Z_G = \int D\phi e^{-H[\phi]} \quad . \tag{4.15}$$

The first term in Eq.(4.14) is the free energy of the pure water solvent. The second term is the energy due to the fixed charge distribution of the membranes and macromolecules. Finally, the fugacity term corresponds to the energy due to the mobile ions. One indeed notes that the integral in the last term is the Boltzmann distribution of a single ion experiencing the potentials $W_i(\mathbf{r})$ and $\phi(\mathbf{r})$.

4.3 Poisson-Boltzmann Equation From the Coulombic Liquid Hamiltonian

In this section, we show that the Poisson-Boltzmann equation corresponds to the mean field (MF) approximation of the Coulombic liquid Hamiltonian functional. As the MF approximation corresponds to the saddle point evaluation of the partition function in Eq.(4.12), we take the functional derivative of the Hamiltonian Eq.(4.14). This yields

$$\frac{\delta H}{\delta\phi(\mathbf{r})} = -i\rho_0(\mathbf{r}) - \sum_{i=1}^{p} iq_i\lambda_i e^{-\beta W_i(\mathbf{r})+iq_i\phi(\mathbf{r})} - \frac{k_B T}{e^2}\nabla\epsilon(\mathbf{r})\cdot\nabla\phi(\mathbf{r}) = 0 \quad . \tag{4.16}$$

Then, via the transformation $\phi \to i\phi$, we pass from the complex to the real electrostatic potential. In the liquid region where $\epsilon(\mathbf{r}) = \epsilon_w$, one finally gets the saddle point equation

$$\nabla^2\phi = -4\pi l_B \left[\sum_{i=\pm} \lambda_i z_i e^{-\beta W_i(\mathbf{r}) - z_i\phi(\mathbf{r})} + \rho_0(\mathbf{r})\right] \quad , \tag{4.17}$$

which is exactly the Poisson-Boltzmann equation (2.8)

4.4 Debye-Hückel-Level Grand Potential

In this section, we evaluate the electrostatic grand potential of the charged system at the Debye-Hückel level. This approach consists of treating the non-linear Hamiltonian (4.14) at the Gaussian level.

First, one should relate the ionic fugacity λ_i to the bulk ion concentration $n_{i,b}$. To this aim, we note that the local particle density is given by the thermodynamic relation

$$n_i(\mathbf{r}) = \lambda_i \frac{\partial \ln Z_G}{\partial \lambda_i} \quad . \tag{4.18}$$

Plugging the partition function (4.13) into Eq.(4.18), one finds

$$n_i(\mathbf{r}) = \lambda_i \langle e^{iz_i\phi(\mathbf{r})} \rangle \quad , \tag{4.19}$$

where the bracket means the field average, i.e.

$$\langle F[\phi] \rangle = \frac{1}{Z_G} \int D\phi e^{-H[\phi]} F[\phi] \quad . \tag{4.20}$$

At this point,we introduce the DH approximation. To this aim, we Taylor-expand the Hamiltonian (4.14) and the ion density (4.19) at the second order in the potential $\phi(\mathbf{r})$. One obtains

$$\begin{aligned} H_0[\phi(\mathbf{r})] \approx & \int d\mathbf{r} \left[\frac{\epsilon(\mathbf{r})}{2\beta e^2}[\nabla\phi(\mathbf{r})]^2 - i\rho_0(\mathbf{r})\phi(\mathbf{r})\right] \\ & - \sum_{i=1}^{p} \lambda_i - \sum_{i=1}^{p} \lambda_i \int d\mathbf{r} \left[iz_i\phi(\mathbf{r}) - \frac{z_i^2}{2}\phi^2(\mathbf{r})\right] \quad , \end{aligned} \tag{4.21}$$

$$n_{i,b}(\mathbf{r}) \approx \lambda_i \left[1 + iz_i\langle\phi(\mathbf{r})\rangle - \frac{z_i^2}{2}\langle\phi^2(\mathbf{r})\rangle\right] \quad . \tag{4.22}$$

Evaluating Eq.(4.22) in the bulk region where the average potential vanishes ($\langle\phi(\mathbf{r})\rangle = 0$), extracting from the latter the ion fugacity λ_i in terms of the bulk concentration $n_{i,b}$ and noting the symmetry of the NaCl solution ($p = 2$), i.e. $z_\pm = \pm 1$ and $n_{\pm,b} = n_b$, Eq.(4.21) becomes

$$\begin{aligned} H_0[\phi(\mathbf{r})] = \int d\mathbf{r} \left[\frac{\epsilon(\mathbf{r})}{2\beta e^2}[\nabla\phi(\mathbf{r})]^2 - i\rho_0(\mathbf{r})\phi(\mathbf{r})\right] \\ -n_b[2 + z^2 v_{DH,b}(0)] + n_b z^2 \int d\mathbf{r}\phi^2(\mathbf{r}) + \frac{n_b}{2} z^4 \int d\mathbf{r} v_{DH}(\mathbf{r},\mathbf{r})\phi^2(\mathbf{r}) \quad , \end{aligned} \tag{4.23}$$

or

$$H_0[\phi(\mathbf{r})] = \int \frac{d\mathbf{r}d\mathbf{r}'}{2}\phi(\mathbf{r})v_{DH}^{-1}(\mathbf{r},\mathbf{r}')\phi(\mathbf{r}') - i\int d\mathbf{r}\rho_0(\mathbf{r})\phi(\mathbf{r}) \quad , \tag{4.24}$$

where we defined the inverse of the DH Green's function

$$v_{DH}^{-1}(\mathbf{r},\mathbf{r}') = -\frac{1}{\beta e^2}\nabla\cdot\epsilon(\mathbf{r})\nabla\cdot\delta(\mathbf{r}-\mathbf{r}') + 2n_b z^2\delta(\mathbf{r}-\mathbf{r}') \quad . \tag{4.25}$$

Substituting now the quadratic Hamiltonian (4.24) into Eq.(4.15), the partition function becomes a Gaussian integral of the potential $\phi(\mathbf{r})$, i.e.

$$Z_0 = \int D\phi e^{-\frac{1}{2}\int d\mathbf{r}d\mathbf{r}'\phi(\mathbf{r})v_{DH}^{-1}(\mathbf{r},\mathbf{r}')\phi(\mathbf{r}') - i\int d\mathbf{r}\rho_0(\mathbf{r})\phi(\mathbf{r})} \quad . \tag{4.26}$$

Using the Hubbard-Stratonovich identity described in Appendix A, the functional integral in Eq.(4.26) can be evaluated exactly. One obtains

$$Z_0 = \det{}^{1/2}[v_{DH}^{-1}(\mathbf{r},\mathbf{r}')]e^{-\frac{1}{2}d\mathbf{r}d\mathbf{r}'\rho_0(\mathbf{r})v_{DH}(\mathbf{r},\mathbf{r}')\rho_0(\mathbf{r}')} \quad . \tag{4.27}$$

Consequently, the electrostatic grand potential defined as $\Omega_{DH} = -k_B T \ln Z_0$ becomes

$$\Omega_G = -k_B T \ln\left(\det{}^{1/2}[v_{DH}(\mathbf{r},\mathbf{r}')]\right) + k_B T \int \frac{d\mathbf{r}d\mathbf{r}'}{2}\rho_0(\mathbf{r})v_{DH}(\mathbf{r},\mathbf{r}')\rho_0(\mathbf{r}') \quad . \tag{4.28}$$

The first term of Eq.(4.28) is the liquid free energy, and the second term corresponds to the polymer total free energy.

Chapter 5

Electrostatic Translocation Model

In this chapter, we introduce the theoretical model of a polymer translocating through a charged membrane. Then, by computing the polymer's grand potential, we evaluate the electrostatic energy landscape of the polymer approach and translocation phases.

5.1 General Formalism

5.1.1 Debye-Hückel Theory of Polymer-Membrane Interactions in The Approach Phase

Fig.(5.1) depicts the polymer-membrane system in the approach phase. A polymer (e.g. DNA) with length L and line charge density $-|\lambda|$ approaches a membrane along the z-axis. The approach occurs from the CIS side with the polymer's right end being at $z = z_t < 0$ [1]. The membrane of thickness d and a relative

[1] It has been previously observed that the DNA modelling as a cylindrical rod is a reasonable approximation. Indeed, according to Holm [21], for a DNA radius $r > 1.5$ nm, all the helical

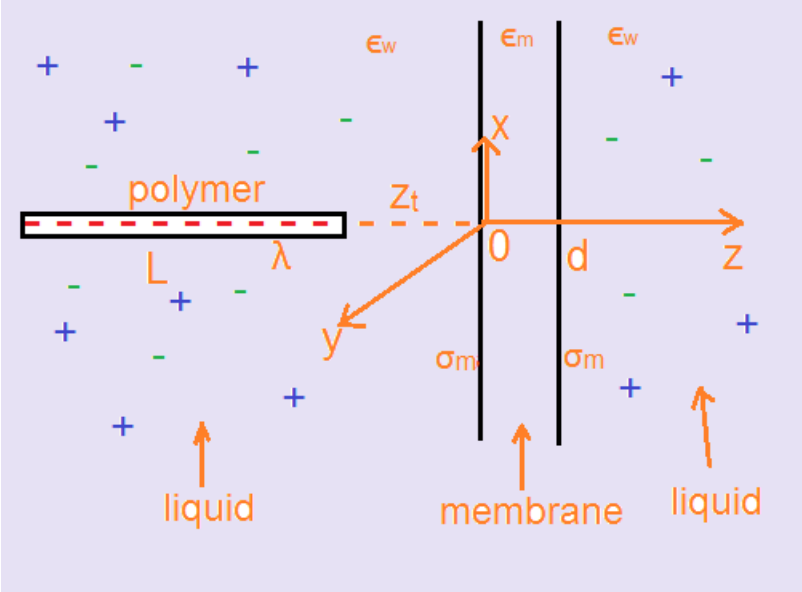

Figure 5.1: Schematic representation of a polymer with length L approaching a membrane of thickness d from the CIS side at a distance z_t ($L >> d$).

permittivity ϵ_m is located in the x-y plane. Both surfaces of the membrane have uniform surface charge density σ_m. The polymer and the membrane are in a symmetric monovalent electrolyte solution with bulk ion concentration n_b and relative permittivity $\epsilon_w = 80$. [2]. The whole system is at room temperature $T = 300°$ K. In our model, we assume $L >> d$.

In Eq.(4.28) of the previous section, the total free energy of the polymer was found to be

$$\Omega_{pol,tot} = k_B T \int \frac{d\mathbf{r}d\mathbf{r}'}{2} \rho_0(\mathbf{r}) v_{DH}(\mathbf{r},\mathbf{r}') \rho_0(\mathbf{r}') \quad , \tag{5.1}$$

where $\rho_0(\mathbf{r})$ stands for the density of the fixed charges as the polymer and the membrane, i.e.

$$\rho_0(\mathbf{r}) = -\lambda \delta(\mathbf{r}_{||}) g(z) + \sigma_m [\delta(z) + \delta(z-d)] \quad , \tag{5.2}$$

with $|\lambda| > 0$. The first term of Eq.(5.2) is the polymer charge density, with the delta function indicating that the polymer is the origin of the x-y plane, and

information disappear. More precisely, a simulation model was run for the ion iso-density surface around the DNA, and it was found that the first layer of ions took a helical shape, while the second layer took a cylindrical shape, indicating that the ions do not sense the helical information for $r > 1.5$ nm.

[2] Permittivities are expressed in units of ϵ_0 such that $\epsilon_0 = 1$.

$g(z)$ stands for the polymer structure factor along the z-axis. The second term of Eq.(5.2) is in turn the charge density of the membrane.
The translational symmetry in the membrane plane implies $v_{DH}(\mathbf{r},\mathbf{r}') \equiv v_{DH}(\mathbf{r}_{||} - \mathbf{r}'_{||}, z, z')$. Thus, one can Fourier expand the Green's function as

$$v_{DH}(\mathbf{r},\mathbf{r}') = \int \frac{d^2\mathbf{k}}{(2\pi)^2} e^{i\mathbf{k}\cdot|\mathbf{r}_{||}-\mathbf{r}'_{||}|} \tilde{v}_{DH}(\mathbf{k},z,z') \quad . \tag{5.3}$$

Substituting Eq.(5.2) and Eq.(5.3) into Eq.(5.1), and subtracting the membrane self energy $\Omega_{mem} \equiv \int \frac{d\mathbf{r}d\mathbf{r}'}{2}\sigma_m(\mathbf{r})v_{DH}(\mathbf{r},\mathbf{r}')\sigma_m(\mathbf{r}')$, the total polymer energy follows as

$$\begin{aligned}\frac{\Omega_{pol,tot}}{k_BT} &= \lambda^2 \int_{-\infty}^{\infty} dz \int_{-\infty}^{\infty} dz' \int_0^{\infty} \frac{dkk}{4\pi} g(z)\tilde{v}_{DH}(k,z,z')g(z') \\ &- \lambda\sigma_m \int_{-\infty}^{\infty} dz g(z)[\tilde{v}_{DH}(k,z,0) + \tilde{v}_{DH}(k,z,d)] \\ &= (\Omega_{pol} + \Omega_{pm})/(k_BT) \quad .\end{aligned} \tag{5.4}$$

The first term of Eq.(5.4) is the polymer self energy induced by the polymer-image charge interactions. The second term is in turn the energy of the polymer-membrane interactions.

5.1.2 Debye-Hückel Theory of Polymer-Membrane Interactions in The Translocation Phase

Fig.(5.2) illustrates the polymer translocation phase. The system has the same description as the previous subsection except that the translocating polymer length on the TRANS side is l_t and on the CIS side is $L - l_t$. It is important to emphasize that based on the assumption $L >> d$, our model neglects the electrostatics of the polymer portion inside the membrane [3].

The dielectric permittivity function is in turn

$$\epsilon(\mathbf{r}) = \epsilon(z) = \epsilon_w\theta(-z) + \epsilon_m\theta(z)\theta(d-z) + \epsilon_w\theta(z-d) \quad , \tag{5.5}$$

[3] This approximation is for analytical simplicity and is valid for $d << L$. However, Green's function for the pore has been calculated in ref [6].

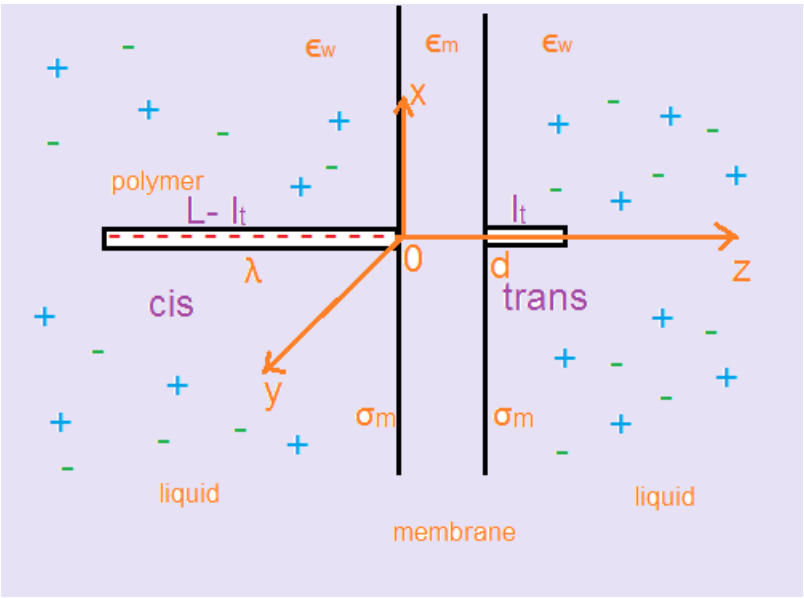

Figure 5.2: Schematic depiction of a polymer with length L translocating through a membrane of thickness d from the CIS to the TRANS side.

where ϵ_w and ϵ_m are the permittivity of water and the membrane, respectively, and $\theta(z)$ stands for the Heaviside step function defined as

$$\theta(z-a) = \{^{1,\ z\geq a}_{0,\ z<a} \quad . \tag{5.6}$$

Subtracting from Eq.(5.4) the bulk part of the polymer grand potential, the polymer self-energy and the polymer-membrane interaction energy follows as

$$\frac{\Delta\Omega_{pol}}{k_BT} = \lambda^2 \int_0^\infty \frac{dkk}{4\pi} \int_{-\infty}^{\infty} dz \int_{-\infty}^{\infty} dz' g(z)\delta\tilde{v}_{DH}(z,z')g(z) \quad , \tag{5.7}$$

$$\Omega_{pm} = -k_BT\lambda \int_{-\infty}^{\infty} dz g(z)\psi_m(z) \quad , \tag{5.8}$$

where $\delta\tilde{v}_{DH}(z,z',k) = \tilde{v}_{DH}(z,z') - \tilde{v}_b(z-z')$ is the Fourier transformed Green's function renormalized by its bulk value, and $\psi_m(z)$ is the electrostatic potential induced by interfacial charge distribution on the membrane walls. The potential $\psi(z)$ solves the DH or the linearized Poisson-Boltzmann equation

$$[\delta_z^2 - \kappa^2\theta(-z)\theta(z-d)]\psi_m(z) = -4\pi l_B\rho_m(z) \quad , \tag{5.9}$$

where the step functions accounts for the absence of charges inside the membrane. Solving Eq.(5.9) with the Gauss' law and the continuity of the potential through

the membrane walls, one finds

$$\psi_m(z) = \frac{2}{\kappa l_G}\left[\theta(-z)e^{\kappa z} + \theta(z)\theta(d-z) + \theta(z-d)e^{\kappa(d-z)}\right] \quad . \tag{5.10}$$

5.2 Polymer Grand Potential in the Approach and Translocation Phases

5.2.1 Approach Phase

In the approach phase displayed in Fig. (5.1), we can write the polymer structure factor as

$$g_{app}(z) = \theta(-z)\theta(z_t - z)\theta(z - z_t + L) \quad . \tag{5.11}$$

Substituting into Eq.(5.7) the structure factor in Eq.(5.11) together with the Green's function $\delta\tilde{v}_{DH}(z, z')$ calculated in Appendix C, the polymer self-energy in the approach phase becomes

$$\frac{\Delta\Omega_{pol,app}}{k_B T} = \frac{\lambda^2 l_B}{2}\int_0^\infty \frac{dkk}{p^3}\frac{\Delta(1-e^{-2kd})}{1-\Delta^2 e^{-2kd}} e^{-2p|z_t|}[1-e^{-pL}]^2 \quad . \tag{5.12}$$

The parameters p and Δ used in Eq.(5.12) have been defined in appendix C. Now, we wish to evaluate the polymer-membrane interaction potential in Eq.(5.8). Using Eqs. (5.10) and (5.11), one obtains

$$\frac{\Delta\Omega_{pm,app}}{k_B T} = -\frac{2}{\kappa l_G} Q_{eff}(L) e^{-\kappa|z_t|} \quad , \tag{5.13}$$

where we defined the effective polymer charge

$$Q_{eff}(L) \equiv \lambda\frac{1-e^{-\kappa L}}{\kappa} \quad . \tag{5.14}$$

5.2.2 Translocation Phase

In this part, we derive the polymer grand potential for the translocation phase illustrated in Fig. 5.2. In this case, the polymer structure factor is

$$g_{trans}(z) = \theta(-z)\theta(z - L + l_t) + \theta(z-d)\theta(d + l_t - z) \quad . \tag{5.15}$$

Inserting Eq.(5.15) into equation (5.7), the polymer self-energy follows as

$$\Delta\Omega_{pol,trans}(l_t) = \Delta\Omega_{intra}(l_t) + \Delta\Omega_{inter}(l_t) \quad , \tag{5.16}$$

where the component

$$\frac{\Delta\Omega_{intra}(l_t)}{k_BT} = \frac{\lambda^2 l_B}{2}\int_0^\infty \frac{dkk}{p^3}\frac{\Delta(1-e^{-2kd})}{1-\Delta^2 e^{-2kd}}\left([1-e^{-p(L-l_t)}]^2 + [1-e^{-pl_t}]^2\right) \quad , \tag{5.17}$$

is the self-interaction of the polymer portions on the TRANS and CIS sides, and

$$\frac{\Delta\Omega_{inter}(l_t)}{k_BT} = -\lambda^2 l_B\int_0^\infty \frac{dkk}{p^3}\left[\frac{(1-\Delta^2)e^{(p-k)d}}{1-\Delta^2 e^{-2kd}} - 1\right] e^{-pd}[1-e^{-pl_t}][1-e^{-p(L-l_t)}] \quad , \tag{5.18}$$

is the coupling energy of the separate TRANS and CIS portions.
Finally, evaluating the polymer-membrane interaction energy (5.8) with Eqs. (5.10) and (5.15), one gets

$$\frac{\Omega_{pm}(l_t)}{k_BT} = -\frac{2}{\kappa l_G}[Q_{eff}(L-l_t) + Q_{eff}(l_t)] \quad , \tag{5.19}$$

where the effective charge has been introduced in equation (5.14).

5.3 The Effect of Tunable Model Parameters on the Approach and Translocation Phases

This section investigates the effect of the membrane permittivity, the salt density, the polymer length, and the membrane charge on the polymer approach and translocation phases.

5.3.1 Membrane Permittivity

In this part, we focus on the effect of the membrane permittivity on the polymer grand potential in the approach and translocation phases through a neutral membrane ($\sigma_m = 0$). The polymer length is $L = 10$ nm, the membrane thickness is $d = 2$ nm, and the solution concentration is $n_b = 0.01$ M. The approach

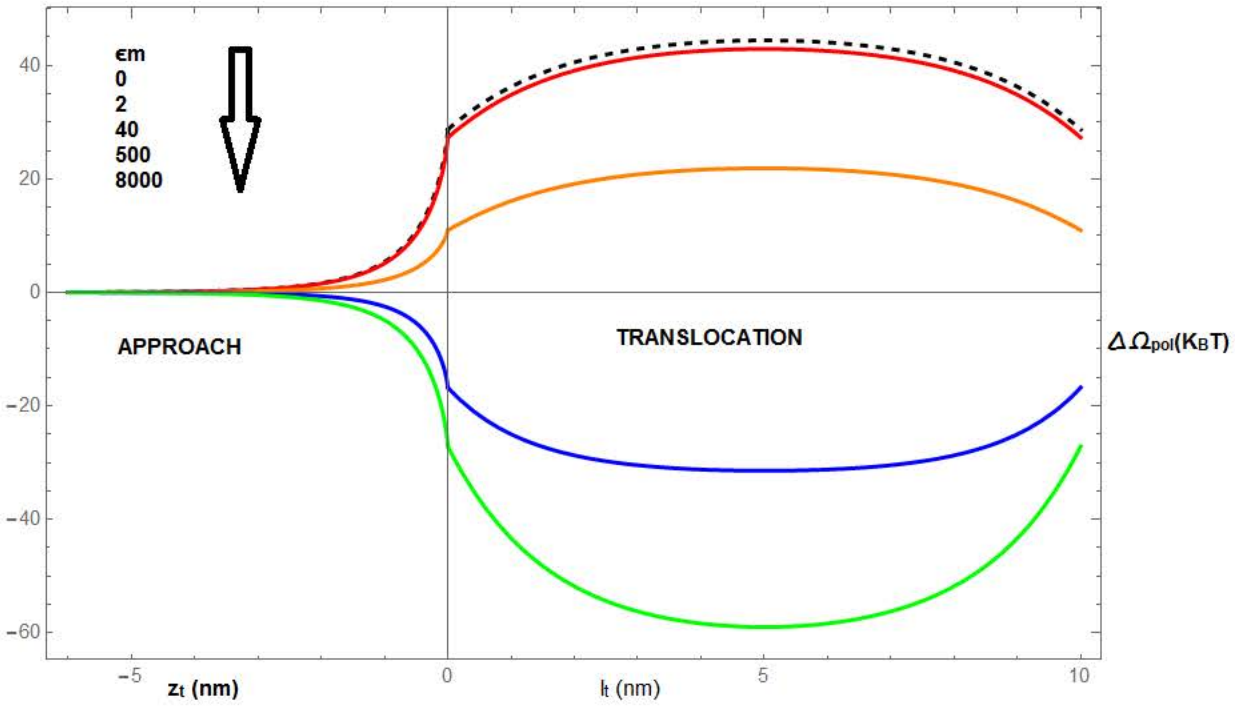

Figure 5.3: Polymer grand potential in the approach and translocation phases through a neutral membrane ($\sigma_m = 0$) for different ϵ_m's. The polymer length is $L = 10$ nm, the membrane thickness is $d = 2$ nm, and the solution concentration is $n_b = 0.01$ M. The black dashed curve corresponds to the limit $\epsilon_m = 0$.

phase is described in terms of the polymer position z_t on the CIS side. Similarly, the translocation is described in terms of the translocated polymer length l_t on the TRANS side, with $0 \leq l_t \leq L$. Commonly, carbon-based membranes have permittivity values around $\epsilon_m = 2$, however, recent membrane engineering technologies have allowed to reach membrane permittivities up to $\epsilon_m = 8000$ [22], [23]. This point is the motivation behind our consideration of permittivity values higher than 2.

In Fig.(5.3), we plotted equations (5.12) in the approach phase and (5.16) in the translocation phase for permittivity values of $\epsilon_m = 2, 40, 500$, and 8000. For $\epsilon_m = 2$, the grand potential initially rises monotonically until it reaches a contact value at the membrane surface $\Delta\Omega_{pol}(z_t = 0) \simeq 27 \;\; k_{\mathrm{B}}T$. In the subsequent translocation phase, it reaches its maximum value of $\Delta\Omega_{tot,trans}(l_t = L/2) \simeq 43 \;\; k_{\mathrm{B}}T$ at half the polymer length $l_t = L/2$, then it decreases reaching the contact value at $l_t = L$: $\Delta\Omega_{tot,trans}(l_t = L) = \Delta\Omega_{pol}(z_t = 0) \simeq 27 \;\; k_{\mathrm{B}}T$.

The contact value for $\epsilon_m = 40$ is seen to be reduced to slightly less than half the value of $\epsilon_m = 2$, i.e. $\Delta\Omega_{pol}(z_t = 0)|_{\epsilon_m=40} \simeq 11 \;\; k_{\mathrm{B}}T$. This indicates that the potential barrier is a result of the interaction of the polymer charges with their electrostatic images.

For permittivity values higher than that of water, the grand potential becomes negative and reaches its minimum at half of the translocation phase. In other words, when the membrane permittivity highly exceeds the water permittivity, the membrane becomes an attraction point for the polymer. In particular, for $\epsilon_m = 8000$, the potential well drops down to $\sim -59 \;\; k_{\mathrm{B}}T$. This result suggests that engineered membranes with high permittivities can trap the polymer for some time.

It is also important to note that in electrophoresis experiments, a constant external electric field is applied, and therefore coupled to the polymer/DNA molecule. This will result in a linearly decreasing potential that will further lower the total grand potential of the polymer.

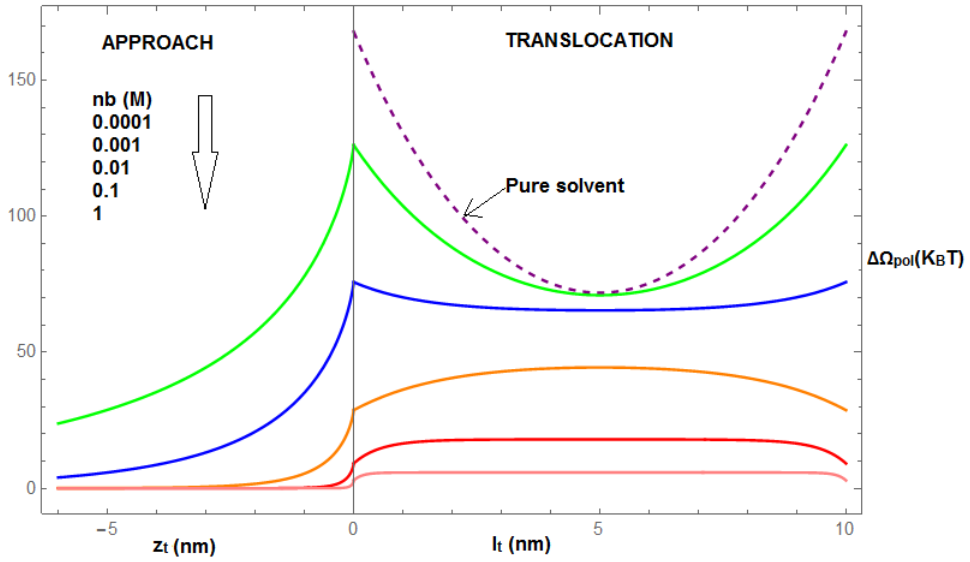

Figure 5.4: Polymer grand potential in the approach and translocation phases through a neutral membrane ($\sigma_m = 0$) for different salt concentrations in the limit of $\epsilon_m = 0$. The polymer length is $L = 10$ nm, and the membrane thickness $d = 2$ nm. The black curve is for the pure solvent limit $n_b = 0$.

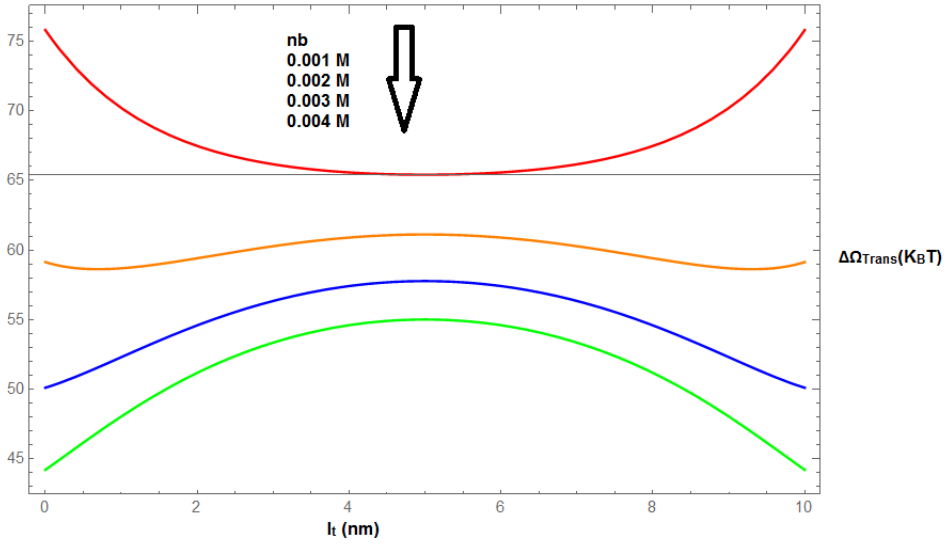

Figure 5.5: Polymer translocation energy for salt concentrations $n_b = 0.001, 0.002, 0.003, 0.004$ M. The figure shows how the translocation energy profile turns from concave to convex at the characteristic concentration $n_b \simeq 0.002$ M.

5.3.2 Salt Concentration

Here, we investigate the effect of the salt concentration -which is an easily tunable parameter- on the electrostatic grand potential of the translocating polymer. For analytical simplicity, we consider the common case of carbon-based low permittivity membranes. Thus, we set the membrane permittivity to $\epsilon_m = 0$ (Fig.(5.3) shows that this is a good approximation of the case $\epsilon_m = 2$). As a result, Eqs. (5.12), (5.17), and (5.18) simplify as

$$\frac{\Delta\Omega_{pol}(z_t)}{k_BT} = \frac{l_B\lambda^2}{2}\int_0^\infty \frac{dkk}{p^3}(1-e^{-pL})e^{-2p|z_t|} \quad , \tag{5.20}$$

$$\frac{\Delta\Omega_{intra}(l_t)}{k_BT} = \frac{l_B\lambda^2}{2}\int_0^\infty \frac{dkk}{p^3}\left([1-e^{-pl_t}]^2+[1-e^{-p(L-l_t)}]^2\right) \quad , \tag{5.21}$$

$$\frac{\Delta\Omega_{inter}(l_t)}{k_BT} = -l_B\lambda^2\int_0^\infty \frac{dkk}{p^3}e^{-pd}[1-e^{-pl_t}][1-e^{-p(L-l_t)}] \quad . \tag{5.22}$$

Carrying out the integrals, one obtains

$$\frac{\Delta\Omega_{pol}(z_t)}{k_BT} = l_B\lambda^2 G(z_t) \quad , \tag{5.23}$$

$$\frac{\Delta\Omega_{intra}(l_t)}{k_BT} = l_B\lambda^2 H(l_t) \quad , \tag{5.24}$$

$$\frac{\Delta\Omega_{inter}(l_t)}{k_BT} = -l_B\lambda^2 F(l_t) \quad , \tag{5.25}$$

where $G(z_t)$, $H(l_t)$, and $F(l_t)$ are auxiliary functions defined as

$$\begin{aligned} G(z_t) = 2|z_t|\left(\Gamma[-1,2\kappa(|z_t|+L)]-2\Gamma[-1,\kappa(2|z_t|+L)]+\Gamma[-1,2\kappa|z_t|]\right)+ \\ 2L\left(\Gamma[-1,2\kappa(|z_t|+L)]-\Gamma[-1,\kappa(2|z_t|+L)]\right) \quad , \end{aligned} \tag{5.26}$$

$$\begin{aligned} H(l_t) = \frac{1}{\kappa}+l_t\left(\Gamma[-1,2\kappa l_t]-\Gamma[-1,\kappa l_t]\right) \\ +(L-l_t)\left(\Gamma[-1,2\kappa(L-l_t)]-\Gamma[-1,\kappa(L-l_t)]\right) \end{aligned} \quad , \tag{5.27}$$

$$F(l_t) = d\Gamma[-1,d\kappa]-(d+L-l_t)\Gamma[-1,\kappa(d+L-l_t)]-(d+l_t)\Gamma[-1,\kappa(d+l_t)]+(d+L)\Gamma[-1,\kappa(d+l)] \quad , \tag{5.28}$$

where

$$\Gamma(s,x) = \int_x^\infty t^{s-1}e^{-t}dt \tag{5.29}$$

is the incomplete Gamma function [4].

Fig.(5.4) displays the polymer grand potential's dependence on the salt concentration. One notices an inverse proportionality between the salt concentration and the potential value at the membrane surface ($z_t = 0$) in the approach phase. Besides, we observe an inverse proportionality between the salt concentration and the smoothness of the potential increase in the approach phase; i.e., for low concentrations, the potential increases smoothly and monotonically in the approach phase, while for relatively high concentrations, the potential increases abruptly near the membrane surface ($z_t = 0$). This behaviour is similar to the behaviour observed in the original article of Ref [5] where charge re-normalization is applied. However, in the translocation phase, the behaviour is quite different. In Fig.(5.4), for relatively high concentrations, the potential increases until it reaches a maximum value at $l_t = L/2 = 5$ nm. The potential then drops and reaches the value at $l_t = L = 10$ nm at the beginning of the translocation phase ($l_t = 0$). Moreover, for low concentrations, the potential starts to decrease after the barrier at $z_t = l_t = 0$ till it reaches a minimum value at $l_t = L/2 = 5$ nm. Then, the potential at $l_t = L = 10$ nm rises and converges again to the potential value at the beginning of the translocation.

Thus, one can conclude that low salt concentration values are more favourable in terms of the translocation energy. This is indeed the observation of the reference paper [5] where the minimum values of the potentials at low concentrations were found to be smaller than their peak for high concentrations. This is however not the case here where the charge re-normalization is not applied. Although the translocation potential exhibits a concave behaviour at low concentrations, its minimum values are significantly larger than the maximum values of the high concentration convex curves. This observation points out the failure of the DH approximation at low salt concentrations. We also observe that at lower salt concentrations, the metastable potential well in the translocation phase becomes

[4]Here, we must note that in the original article reproduced here [5], the solutions are expressed in terms of the exponential integral functions $Ei(x)$. To test whether the two expressions are equivalent, I evaluated both of them at the same points, but they returned slightly different values in the energies of the translocation phase, and this discrepancy increased with lower values of salt concentration. Thus, I evaluated the original energy expressions ((5.12), (5.17), (5.18)) -while giving the software $\epsilon_m = 0$ as one of the inputs- at the same points, and it returned the same values as the solutions with the Gamma functions. Therefore, I decided to continue my calculations using the Gamma function solution.

deeper until it reaches its minimum in the pure solvent limit (i.e. $n_b \to 0$ and $\kappa \to 0$) where the grand potential components take the simple form

$$\frac{\Delta\Omega_{intra}(l_t)}{k_BT} = l_B L\lambda^2 \ln(2) \quad , \tag{5.30}$$

$$\begin{aligned}\frac{\Delta\Omega_{inter}(l_t)}{k_BT} = -l_B\lambda^2 \left(d\ln\left[\frac{2(d+L)}{(d+l_t)(d+L-l_t)}\right] + L\ln\left[\frac{d+L}{d+L-l_t}\right]\right) \\ -l_B\lambda^2 l_t \ln\left[\frac{d+L-l_t}{d+l_t}\right] \quad .\end{aligned} \tag{5.31}$$

[5] Eqs (5.30) and (5.31) are plotted in Fig.(5.4) as the dashed curve. The deeper potential well in the salt-free liquid implies that in pure solvents, one can trap the polymer for longer periods of time. As the challenge in polymer translocation consists in lowering the DNA velocity, this is a key result of the model. This result also means that one can control the polymer velocity via tuning the salt concentration.

The emergence of an attractive potential well at low salt concentrations despite the presence of the image-charge repulsion seems counter-intuitive. To clarify this point, we probe the competition between the attractive trans-cis and repulsive image-charge interactions mediated by the dielectric membrane. According to Eq.(5.16), the net electrostatic force on the polymer $F_{tot}(l_t) = -d\Delta\Omega_{tot}(l_t)/dt$ can be decomposed as $F_{tot}(l_t) = F_{intra}(l_t) + F_{inter}(l_t)$, where the force components are

$$\begin{aligned}\frac{F_{intra}(l_t)}{k_BTl_B\lambda^2} = -\frac{e^{-\kappa(L-l_t)}(e^{-\kappa(L-l_t)}-2)}{2\kappa(L-l_t)} - \frac{e^{-2\kappa l_t}(2e^{\kappa l_t}-1)}{2\kappa l_t} \\ -\Gamma[-1,\kappa(L-l_t)] + \Gamma[-1,2\kappa(L-l_t)] \\ +\Gamma[-1,\kappa l_t] - \Gamma[-1,2\kappa l_t] \quad ,\end{aligned} \tag{5.32}$$

$$\frac{F_{inter}(l_t)}{k_BTl_B\lambda^2} = \frac{e^{-\kappa(d+l_t)}}{\kappa(d+l_t)} - \frac{e^{-\kappa(d+L-l_t)}}{\kappa(d+L-l_t)} + \Gamma[-1,\kappa(d+L-l_t)] - \Gamma[-1,\kappa(d+l_t)] \quad . \tag{5.33}$$

In Fig.(5.4), the characteristic salt concentration where the polymer translocation potential turns from convex to concave corresponds to the point where the total electrostatic force turns from negative to positive, i.e. $F_{tot}(l_t = 0) = F_{intra}(l_t =$

[5] This is obtained from the Taylor expansion around $\kappa = 0$.

$0) + F_{inter}(l_t = 0) > 0$. Considering the limit $\kappa L >> 1$ for the sake of simplicity, we find that this occurs when $e^{-\kappa d}/(\kappa d) - \Gamma[-1, \kappa d] > \ln(2)$, or

$$\kappa \gtrsim \frac{0.4}{d} \quad . \tag{5.34}$$

The inequality (5.34) indicates that the thicker the membrane, the lower the critical salt density where the potential turns from unstable to metastable. This can be explained by the fact that a thicker membrane is characterized by stronger repulsive image-charge interactions. For $l_B = 7$Å and $d = 2$ nm, this turnover takes place at the critical salt density $n_b \simeq 0.002$ M (Fig. 5.5).

The emergence of the potential trap via salt reduction can be explained by the fact that in the pure solvent limit, the repulsive image-charge force vanishes $F_{intra} = 0$, and the trans-cis force becomes

$$F_{inter}(l_t) = k_B T l_B \lambda^2 \ln\left[\frac{d + L - l_t}{d + l_t}\right] \quad . \tag{5.35}$$

Hence, in the pure solvent limit, the translocation phase is governed solely by the attractive trans-cis force.

5.3.3 Polymer Length

This section investigates the effect of the polymer length on the polymer grand potential in the translocation phase. First, we focus on the variation of the grand potential as one increases the solution concentration from 0.002 M to 0.004 M. We note in passing that in Fig.(5.6), we plotted the polymer energies rescaled by the characteristic energy $\Delta\Omega^* = k_B T l_B \lambda^2/\kappa$, versus the translocation coordinate rescaled by the polymer length L. For $n_b = 0.002$ M (red curve), the translocation energy has two metastable minima that disappear at higher concentrations $n_b = 0.003$ M (orange curve) and $n_b = 0.004$ M (blue curve). The variation of the energy landscape from the orange to the red curve also suggests that at lower concentrations, the two minima will move closer to each other, and the curve will turn from convex to concave. In addition, the figure shows that as the salt

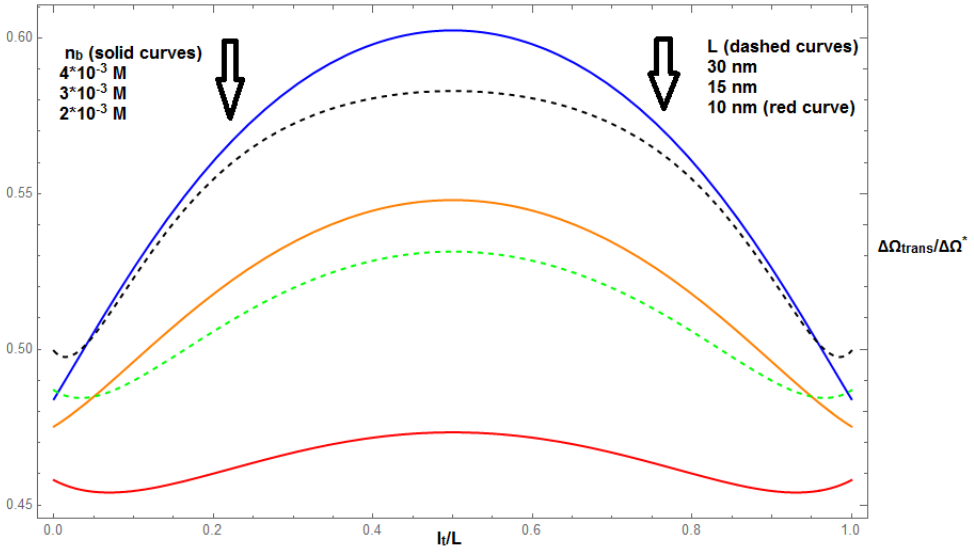

Figure 5.6: Polymer translocation energy rescaled by the characteristic energy $\Delta\Omega^* = k_B T l_B \lambda^2/\kappa$ versus the translocated length rescaled by the polymer length l_t/L. The solution concentration is $n_b = 2 \times 10^{-3}$ M (red curve), $n_b = 3 \times 10^{-3}$ M (orange curve), and $n_b = 4 \times 10^{-3}$ M (blue curve). The polymer length is $L = 10$ nm (red curve), $L = 15$ nm (green curve), and $L = 30$ nm (black curve).

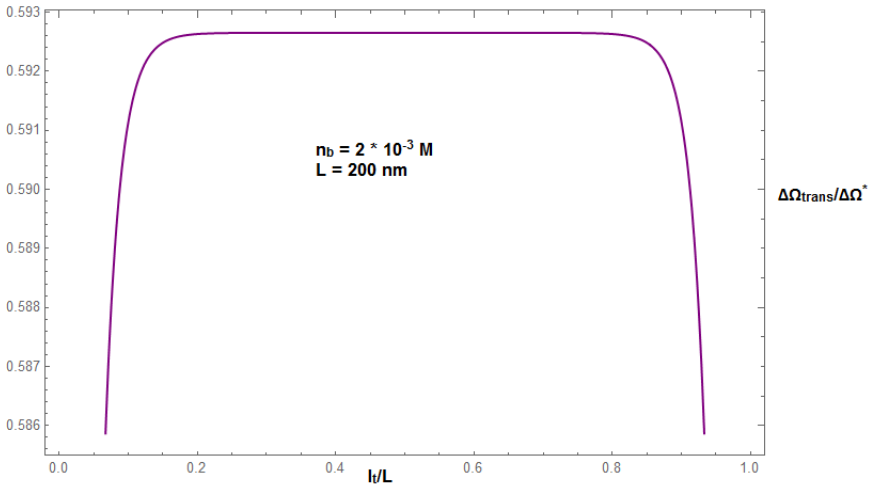

Figure 5.7: Polymer translocation energy rescaled by the characteristic energy $\Delta\Omega^* = k_B T l_B \lambda^2/\kappa$ versus the translocated length rescaled by the polymer length l_t/L. For very long polymers (e.g $L = 200$ nm), the potential curve becomes steep on the sides and the potential has a stable maximum for most of the range $0 < l_t < L$, instead of a metastable point, making the potential curve look like a potential step rather than a convex curve.

concentration increases, the two minima move away from each other until they vanish, and the energy peak at $l_t = L/2 = 5$ nm rises.

Now, we set the concentration value to $n_b = 0.002$ M and vary the polymer length from $L = 10$ nm to $L = 30$ nm (solid red and dashed curves). One notes that the polymer length increase is qualitatively equivalent to the increase of the salt concentration; one indeed sees that the grand potential peak increases with the polymer length L. One also sees that upon increasing the polymer length, the grand potential wells move away from each other towards the edges at $l_t = 0$ and $l_t = L$. The corresponding variation of the translocation energy with the polymer length is due to the polymer self-energy increase with respect to the trans-cis interaction energy. As a result, the longer the polymer is, the steeper the grand potential curve becomes on the sides of the peak. Moreover, for longer polymers, the potential exhibits a stable maximum for most of the range $0 < l_t < L$, instead of a metastable point, making the potential curve look like a potential step (Fig. 5.7) rather than a convex curve (Fig. 5.6). This implies that the electrostatic cost for the translocation of the polymer increases with its length.

5.3.4 Membrane Charge

This part deals with the translocation of the polymer through a charged membrane in the limiting case $\epsilon_m = 0$. We study the effect of the membrane surface charge density on the polymer grand potential in Eq.(5.4). From Eq's (5.13) and (5.23), the polymer grand potential in the approach phase follows

$$\frac{\Delta\Omega_{pol}(z_t)}{k_BT} = l_B\lambda^2 G(z_t) - \frac{2}{\kappa l_G} Q_{eff}(L) e^{-\kappa|z_t|} \quad . \tag{5.36}$$

Then, using Eqs. (5.19), (5.27), and (5.28), the polymer grand potential in the translocation phase can be expressed as

$$\frac{\Delta\Omega_{pol}(l_t)}{k_BT} = l_B\lambda^2[H(l_t) - F(l_t)] - \frac{2}{\kappa l_G}[Q_{eff}(L - l_t) + Q_{eff}(l_t)] \quad . \tag{5.37}$$

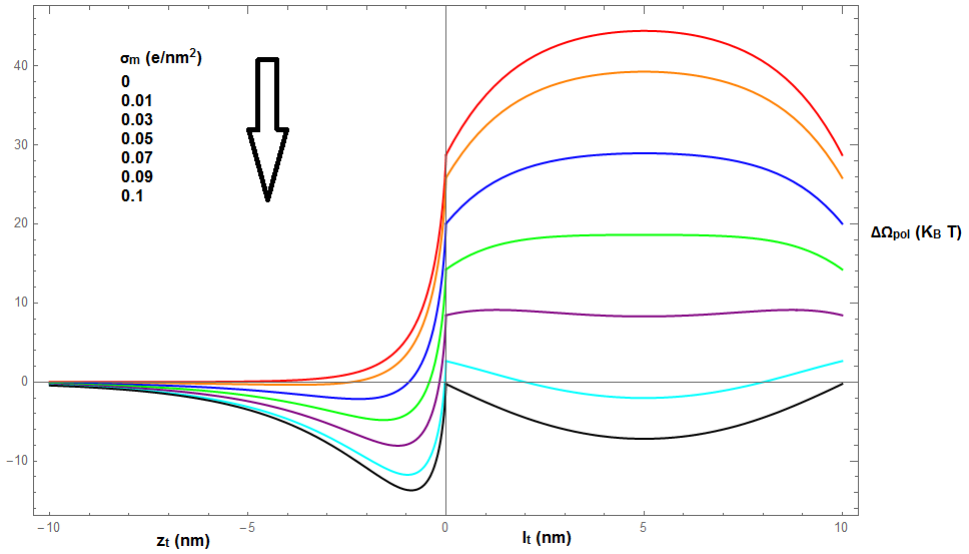

Figure 5.8: Polymer grand potential in the approach and translocation phases for different membrane surface charge densities. The membrane permittivity ϵ_m is set to zero, and the salt concentration is $n_b = 0.01$ M.

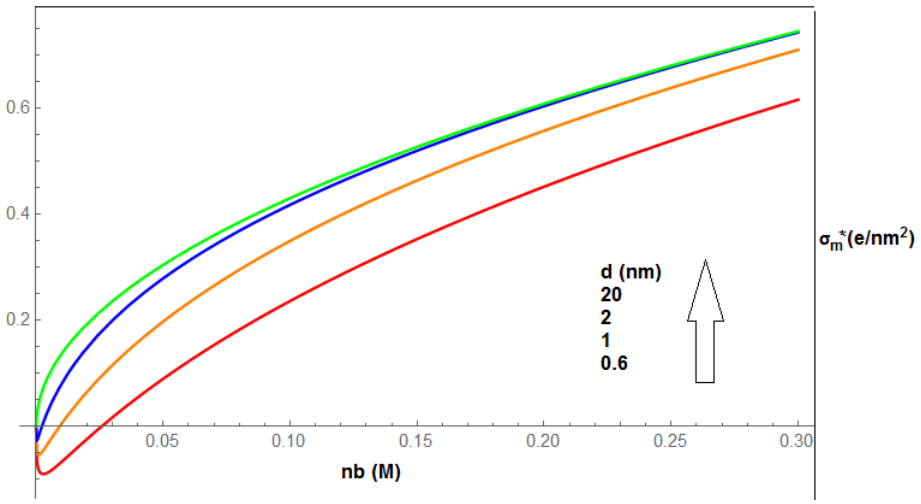

Figure 5.9: The critical membrane surface charge density versus the solution concentration for different membrane thickness values.

We set the solution concentration to $n_b = 0.01$ M. The red curve in Fig.(5.8) shows that due to the polymer-image charge interactions, the polymer translocating through a neutral membrane experiences a repulsive energy barrier. Increasing the membrane charge to $\sigma_m = 0.03 \;\; e/\text{nm}^2$ (blue curve), the potential barrier in the translocation phase decreases. However, in the approach phase, a potential trap appears at $z_t \simeq -2$ nm. This indicates that for charged membranes, the polymer gets trapped near the membrane wall. Increasing further the membrane charge, the potential barrier in the translocation phase drops and switches to a metastable potential trap at $\sigma_m = 0.08 \pm 0.01 \;\; e/\text{nm}^2$ (purple and cyan curves). Going up to $0.1 \;\; e/\text{nm}^2$, both the potential traps in the approach and translocation phases become deeper.
These results suggest that the tuning of the membrane charge can make the membrane an attractive well, enabling the polymer's trapping inside the nanopore.

We now evaluate the critical membrane charge density where the translocation potential at $l_t = L/2$ turns from a maximum to a minimum. This task can be achieved by calculating the electrostatic force from Eq.(5.37), and setting its surface limit to zero, i.e. $F_{tot}(l_t = 0) = 0$. Taking the long polymer limit $\kappa L \to \infty$, the characteristic surface charge density for which the slope of the grand potential turns from positive to negative follows as

$$\sigma_m^* = \frac{\kappa\lambda}{4\pi}\left(\ln(2) + \Gamma[-1,\kappa d] - \frac{e^{-\kappa d}}{\kappa d}\right) \quad . \tag{5.38}$$

[6] The first term in Eq.(5.38) corresponds to the repulsive image-charge interaction, while the remaining terms correspond to the attractive trans-cis interaction. In Fig.(5.9), we plotted the characteristic surface charge density versus the bulk salt concentration n_b for different membrane thickness values. One sees that at low concentration values, the characteristic charge density is negative and drops with increasing concentration until it reaches a minimum. Then, σ_m^* increases monotonically with the salt concentration and turns to positive.

The non-monotonic behavior of Eq.(5.38) can be explained in terms of the

[6] $Ei(-x) = \Gamma[-1,x] - \frac{e^{-x}}{x}$.

competition between the repulsive image-charge and the attractive trans-cis interactions. First, we focus on the high bulk concentration regime $\kappa d >> 1$. In Eq.(5.38), one sees that the last two terms vanish at high bulk ion concentrations. As a result, only the repulsive image-charge attraction survives. Moreover, in the same high ion concentration regime, the larger the salt concentration, the higher the characteristic surface charge density needed for the membrane-polymer attraction to overcome the polymer-charge repulsion. This is due to the fact that at high ion concentrations, the salt screening weakens the field induced by the membrane charges, explaining the positive slope of the critical charge density in Fig.(5.9) at high ion concentrations. Fig.(5.9) also shows that the critical charge density rises with the membrane thickness at fixed salt concentration. This peculiarity stems from the fact that thicker membranes amplify the image-charge repulsion.

We now focus on to the dilute regime $\kappa d << 1$ of Fig.(5.9) where the critical membrane charge density exhibits a non-monotonic behavior. In section 5.3.2, we found that in weak electrolytes, the attractive trans-cis interaction takes over the repulsive image-charge interaction. This need for a negative charge density to compensate for the resulting attractive force leads to the negative value of the critical charge density in Fig.(5.9).
For an analytical insight, we expand Eq.(5.38) around $\kappa = 0$. This yields

$$\sigma_m^* = \frac{\kappa\lambda}{4\pi}[\gamma + \ln(2\kappa d)] \quad , \tag{5.39}$$

where γ is the Euler gamma function. By differentiating Eq.(5.39) with respect to κ, and setting the result to zero, the screening parameter value minimizing σ_m^* follows as

$$\kappa_c = \frac{e^{-1-\gamma}}{2d} \quad . \tag{5.40}$$

Substituting Eq.(5.40) back into Eq.(5.39), the minimum critical membrane charge density becomes

$$\sigma_m^*|_{\kappa_c} = -\frac{\lambda}{8\pi d}e^{-1-\gamma} \quad . \tag{5.41}$$

Eq.(5.41) confirms the negative sign of the minimum critical charge density. The same equality also ascertains that the larger the membrane thickness, the weaker

the critical surface charge density and salt ion concentrations of the the potential reversal.

Chapter 6

Conclusions and Outlook

The polymer grand potential of Eq.(5.7) displays a quadratic dependence on the DNA bare line charge density λ, and the polymer-membrane interaction potential of Eq.(5.8) displays a linear dependence on the membrane surface charge density σ_m. This comes from the DH approximation, which allows for analytical simplicity. In the case of weekly charged membranes, the DH approximation holds and works just fine, but in the case of a strong charged electrolyte like the ds-DNA with bare line charge density $\lambda = 2e/(0.34\text{ nm})$ or a diluted solution with bulk concentration $n_b \lesssim 0.01$ M, the DH approximation is known to overestimate the values of the electrostatic interaction. This might stem from the accumulation of counter-ions around the ds-DNA, reducing the effect of its charge. Hence, in the article by Büyükdağlı *et al.* [5], the variational charge renormalization approach from the article [24] was used, and the effective DNA line charge density was found to be $\tilde{\lambda} = 1/l_B$. Upon replacing the bare DNA charge density with the effective one, the results and figures in the article [5] show a significant discrepancy compared to the results of this thesis.

In the case of a neutral membrane, the dielectric discrepancy between the membrane and the solution significantly affects the electrostatic potential because of the image-charge interaction. For low permittivity carbon-based membranes, the

membrane exhibits a significant repulsive barrier, while in the case of engineered membranes with permittivity that significantly exceeds the water permittivity $\epsilon_m > \epsilon_w$, the membrane becomes an attractive point for the polymer. During translocation, the polymer's grand potential is governed by the repulsive image-charge effect between the polymer and the dielectric membrane and the attractive trans-cis side interaction. In the case of a dilute salt, or a short polymer, the attractive trans-cis side dominates over the repulsive image-charge effect, causing the membrane to act as a metastable point for the polymer, which leads the polymer to spend some time in the pore. This is a big advantage for translocation experiments since their quality increase with the polymer translocation time [25]. In weakly charged membranes, the membrane charge attraction wins over the image-charge repulsion, which leads to an attractive minimum at $z_t \approx -1$ nm followed by a repulsive barrier at $l_t = L/2$. Thus, a polymer approaching a weakly charged membrane will be trapped outside. On the other hand, for stronger membrane charges, the attractive well turns to a metastable point followed by an attractive, stable well. This way, tuning the membrane charge density can be an alternative method interchangeable with tuning the salt concentration for trapping the polymer in the translocation phase for longer times.

One of the main limitations of this model is that the membrane charge density is at the DH level. For this reason, the calculations were restricted to weakly charged membranes. One more thing is the restriction on using only monovalent electrolytes since the PB Eq. is known to break down for multivalent electrolytes or even monovalent electrolytes in low dielectric solvents [6]. Further research that considers changes to the theoretical model will allow for multivalent electrolytes or strongly charged membranes.

It is noteworthy to state that theoretical models, in general, have a variety of limitations; some of them were considered in this work and a lot more in other research studying the current parameters or others. Moreover, technological advancement to solve the current limitations are creating other limitations on the way. For example, the mono-atomic graphene-based membranes succeeded in

solving the thickness problem, which used to affect the accuracy of sequencing due to the presence of more than one nucleotide at a time in the pore since their thickness is significantly smaller than a nucleotide. Thin membranes also allowed us to exclude the polymer's portion inside the pore in our theoretical models, which gave way to more analytical simplicity. However, thin graphene membranes are soft and flexible, making them prone to vibration or deformation upon any thermal or elastic fluctuation [4]. This new problem challenges the solid assumption of theoretical models that both the membrane and the pore are immobile. In their 2016 study, Menais *et al.* approached these membrane vibration effects, which, as they stated, can affect the polymer translocation time [4].

Limitations on theoretical models happen to be not only spatial but temporal as well. In experiments, a base usually spends about 1 μs inside the pore. However, for a better resolution in current measurements, it would be required that the base occupation time be reduced to 1 ms [4].

Research studies approaching the problem of time and transport velocity are quite a lot. One of the methods studied to reduce the translocation velocity is modifying the electrolyte solution, either by adding trivalent Spermidine [15], or large amounts of Lithium salts [4]. In their 2014 paper, Büyükdağlı *et al.* found that the addition of multivalent counter-ions like trivalent Spermidine or quadrivalent Spermine molecules to the solution results in the inversion of polymer charge, which stops the translocation of the polymer and even reverse its motion. They reasoned that this mechanism would minimize the polymer translocation velocity, hence improving the DNA sequencing [15].

Last but not least, the polymer length is a parameter that can have consequential effects. In this work, the limit of a long polymer was considered briefly. A paper by Büyükdağlı *et al.* in 2019 also considered this limit [26]. Such attempts considering the long polymer limit can significantly improve current sequencing methods since nearly all of them can handle the DNA only in small, short fragments.

Bibliography

[1] D. B. JOHN J. KASIANOWICZ, ERIC BRANDIN and D. W. DEAMER, "Characterization of individual polynucleotide molecules using a membrane channel," *Proceedings of the National Academy of Sciences of the United States of America*, vol. 93, no. 24, pp. 13770–13773, 1996.

[2] A. Meller, "Dynamics of polynucleotide transport through nanometre-scale pores," *Journal of Physics: Condensed Matter*, vol. 15, no. 17, p. R581–R607, 2003.

[3] T. A.-N. Vladimir V. Palyulin and R. Metzler, "Polymer translocation: the first two decades and the recent diversification," *Soft Matter*, vol. 10, pp. 9016–9037, 2014.

[4] S. M. Timothée Menais and A. Buhot, "Polymer translocation through nanopores in vibrating thin membranes," *Scientific Reports*, vol. 6, no. 38558, 2016.

[5] S. Buyukdagli and T. Ala-Nissila, "Electrostatics of polymer translocation events in electrolyte solutions," *The Journal of Chemical Physics*, vol. 145, no. 1, 2016.

[6] Y. Levin, "Electrostatics of ions inside the nanopores and trans-membrane channels," *EuroPhysics Letters*, vol. 76, no. 1, pp. 163 – 196, 2006.

[7] A. B. Kolomeisky, "How polymers translocate through pores: Memory is important," *Biophysical Journal*, vol. 94, no. 5, p. 1547–1548, 2008.

[8] D. K.Lubensky and D. R.Nelson, "Driven polymer translocation through a narrow porel," *Biophysical Journal*, vol. 77, no. 4, pp. 1824–1838, 1999.

[9] W. H. Coulter, "Means for counting particles suspended in a fluid," October 1953.

[10] R. W. DeBlois and C. P. Bean, "Counting and sizing of submicron particles by the resistive pulse technique," *Review of Scientific Instruments*, vol. 41, 1970.

[11] I. V. S. M. Bezrukov and V. A. Parsegian, "Counting polymers moving through a single ion channel," *Nature*, vol. 370, pp. 279–281, 1994.

[12] D. Andelman, "Introduction to electrostatics in soft and biological matter," 2004.

[13] W. Sung and P. J. Park, "Polymer translocation through a pore in a membrane," *Physical Review Letters*, vol. 77, no. 4, pp. 783–786, 1996.

[14] S. Buyukdagli and T. Ala-Nissila, "Electrostatic energy barriers from dielectric membranes upon approach of translocating dna molecules," *The Journal of Chemical Physics*, vol. 144, no. 084902, 2016.

[15] S. Buyukdagli and T. Ala-Nissila, "Controlling polymer translocation and ion transport via charge correlations," *Langmuir*, vol. 30, no. 43, pp. 12907–12915, 2014.

[16] D.G.Levitt, "Electrostatic calculations for an ion channel. i. energy and potential profiles and interactions between ions," *Biophysical Journal*, vol. 22, pp. 209–219, 1978.

[17] M. Gouy, "Sur la constitution de la charge électrique à la surface d'un électrolyte," *Journal de Physique*, vol. 9, no. 1, pp. 457–468, 1910.

[18] D. L. Chapman, "A contribution to the theory of electrocapillarity," *The London, Edinburgh, and Dublin Philosophical Magazine and Journal of Science*, vol. 25, no. 148, pp. 475–481, 1913.

[19] P. Debye and E. Hückel, "Zur theorie der elektrolyte. i. gefrierpunktserniedrigung und verwandte erscheinungen," *Physikalische Zeitschrif*, vol. 24, pp. 185–206, 1923.

[20] R. R. Netz and H. Orland, "Beyond poisson-boltzmann: Fluctuation effects and correlation functions," *The European Physical Journal E*, vol. 1, pp. 203–214, 2000.

[21] C. Holm, "How to model dna translocation through nanopores – a multiscale simulational exploration." Physics Colloquim, 2018.

[22] Y. Y. Q. Z. Z.-M. Dang, L. Wang and Q. Lei, "Giant dielectric permittivities in functionalized carbon-nanotube/ electroactive-polymer nanocomposites," *Advanced Materials*, vol. 19, no. 6, pp. 852 – 857, 2007.

[23] B. G. K. O. B. C. L. K. E. J. R. Ayrat Dimiev, Dante Zakhidov and J. M., "Permittivity of dielectric composite materials comprising graphene nanoribbons. the effect of nanostructure," *ACS Applied Materials and Interfaces*, vol. 5, no. 15, pp. 7567–7573, 2013.

[24] R. R. Netz and H. Orland, "Variational charge renormalization in charged systems," *The European Physical Jornal E*, vol. 11, pp. 301–311, 2003.

[25] L. J. A. P. S. R. James Clarke, Hai-Chen Wu and H. Bayley, "Continuous base identification for single-molecule nanopore dna sequencing," *Nature Nanotechnology*, vol. 4, pp. 265–270, 2009.

[26] J. S. Sahin Buyukdagli and T. Ala-Nissila, "Theoretical modeling of polymer translocation: From the electrohydrodynamics of short polymers to the fluctuating long polymers," *Polymers (Basel)*, vol. 11, no. 1, 2019.

Appendix A

Hubbard-Stratonovich Transformation

The Hubbard-Stratonovich (HS) transformation allows to convert a particle theory to its respective field theory by linearising the density operator in the many-body interaction term of the Hamiltonian via the introduction of an auxiliary scalar field. This approach enables to reformulate a system of particles interacting through two-body potentials into a system of independent particles interacting with a fluctuating background field.

In order to derive the HS transformation, we will evaluate the canonical partition function of a one-dimensional Gaussian model $Z_J = \int D\phi e^{-\beta H[\phi]}$, with the Hamiltonian corresponding to a general quadratic functional of the fluctuating potential $\phi(x)$

$$H[\phi(x)] = \frac{1}{2}\int dxdy\phi(x)G^{-1}(x-y)\phi(y) - \int dxJ(x)\phi(x) \quad , \tag{A.1}$$

where $G^{-1}(x-y)$ is the inverse Green's function, and $J(x)$ is an external current or a generating function.
First, we expand the functions in the Hamiltonian (A.1) in the discrete Fourier

space

$$\begin{aligned}
\phi(x) &= \frac{1}{V}\sum_{k_1}\tilde{\phi}(k_1)e^{-ik_1x} \ , \\
\phi(y) &= \frac{1}{V}\sum_{k_2}\tilde{\phi}(k_2)e^{-ik_2y} \ , \\
J(x) &= \frac{1}{V}\sum_{k_3}\tilde{J}(k_3)e^{-ik_3x} \ , \\
G^{-1}(x-y) &= \frac{1}{V}\sum_{k_4}\tilde{G^{-1}}(k_4)e^{-ik_4(x-y)} \ .
\end{aligned} \tag{A.2}$$

Plugging the Fourier expanded functions (A.2) into Eq.(A.1), the Hamiltonian becomes

$$\begin{aligned}
H[\phi(x)] = \frac{1}{2V^3}\sum_{k_1,k_2,k_4}\tilde{\phi}(k_1)\tilde{G^{-1}}(k_4)\tilde{\phi}(k_2)\int dx e^{-i(k_1+k_4)x}\int dy e^{-i(k_2-k_4)y} \\
-\frac{1}{V^2}\sum_{k_1,k_3}\tilde{J}(k_3)\tilde{\phi}(k_1)\int dx e^{-i(k_1+k_3)x} \ .
\end{aligned} \tag{A.3}$$

Next, we make use of the Fourier transformation of the Dirac delta function, i.e. $\tilde{\delta}(k-k') = \frac{1}{V}\int e^{i(k-k')x}$. Eq.(A.3) simplifies to

$$H[\phi(x)] = \frac{1}{2V}\sum_{k}\tilde{\phi}(-k)\tilde{G^{-1}}(k)\tilde{\phi}(k) - \frac{1}{V}\sum_{k}\tilde{J}(-k)\tilde{\phi}(k) \ . \tag{A.4}$$

At this point, we note that the functional integral is defined as the integration over all possible values of the potential function, i.e.

$$Z_J = \int D\phi e^{-\beta H[\phi(x)]} = \prod_x \int d\phi e^{-\beta H[\phi(x)]} \ . \tag{A.5}$$

As the Hamiltonian has been expanded in the Fourier space, the integration measure should be also Fourier transformed. Z_J becomes

$$Z_J = \prod_{k=-\infty}^{\infty}\int d\tilde{\phi}(k)e^{-\beta H[\tilde{\phi}(k)]}\frac{e^{-ikx}}{V} \ . \tag{A.6}$$

In the Hamiltonian (A.4), the modes $\tilde{\phi}(k)$ and $\tilde{\phi}(-k)$ are still coupled. In order to decouple these modes, we decompose the Fourier expanded potential into its real and imaginary components as $\tilde{\phi}(k) = \tilde{\phi_{re}}(k) + i\tilde{\phi_{im}}(k)$. Fourier-transforming

as well the functions $J(x)$ and $G^{-1}(x-y)$, and plugging the Fourier-expanded functions into Eq.(A.4), one obtains

$$\begin{aligned} H[\phi(x)] = \frac{1}{2V}\tilde{\phi}^2(0)\tilde{G}^{-1}(0) - \frac{1}{V}\tilde{\phi}(0) \\ +\frac{1}{V}\sum_{k>0}^{\infty}\left[\tilde{G}^{-1}(k)\tilde{\phi}^2_{re}(k) - 2\tilde{J}_{re}(k)\tilde{\phi}_{re}(k)\right] \\ +\frac{1}{V}\sum_{k>0}^{\infty}\left[\tilde{G}^{-1}(k)\tilde{\phi}^2_{im}(k) - 2\tilde{J}_{im}(k)\tilde{\phi}_{im}(k)\right] \quad . \end{aligned} \tag{A.7}$$

Now, we also have to write the differential element of equation (A.6) in terms of the real and imaginary elements. Using the identity $d\tilde{\phi}(k)d\tilde{\phi}(-k) = |J|d\tilde{\phi}_{re}(k)d\tilde{\phi}_{im}(k)$, where $J=2$ is the Jacobian of the transformation, the partition function (A.6) becomes

$$\begin{aligned} Z_J &= \int_{-\infty}^{\infty} D\tilde{\phi}e^{-\beta H[\tilde{\phi}]} \\ &= 2\int_{-\infty}^{\infty}\frac{1}{V}d\tilde{\phi}(0)\prod_{k>0}\int_{-\infty}^{\infty}\frac{e^{-ikx}}{V}\tilde{\phi}_{re}(k)\int_{-\infty}^{\infty}\frac{e^{-ikx}}{V}\tilde{\phi}_{im}(k)e^{-\beta H[\tilde{\phi}]} \quad . \end{aligned} \tag{A.8}$$

In Eq.(A.8), one notes that the partition function transformed into the product of decoupled Gaussian integrals. Evaluating the latter, the partition function becomes $Z = Z_0 Z_{re} Z_{im}$, where

$$Z_0 = \frac{2}{V}\sqrt{\frac{2\pi V}{\beta\tilde{G}^{-1}(0)}}e^{\frac{\beta\tilde{J}^2(0)}{2V\tilde{G}^{-1}(0)}} \quad , \tag{A.9}$$

$$Z_{re} = \prod_{k>0}\frac{e^{-ikx}}{V}\sqrt{\frac{\pi V}{\beta\tilde{G}^{-1}(0)}}e^{\frac{\beta\tilde{J}^2_{re}(k)}{V\tilde{G}^{-1}(k)}} \quad , \tag{A.10}$$

$$Z_{im} = Z_{re}|_{re\to im} \quad . \tag{A.11}$$

Thus, the partition function can be expressed as

$$Z_J = \frac{2}{V}\sqrt{\frac{2\pi V}{\beta\tilde{G}^{-1}(0)}}e^{\frac{\beta\tilde{J}^2(0)}{2V\tilde{G}^{-1}(0)}}\prod_{k>0}\frac{e^{-ikx}}{V}\sqrt{\frac{\pi V}{\beta\tilde{G}^{-1}(k)}}e^{\sum_k\frac{\beta\tilde{J}^2_{re}(k)}{V\tilde{G}^{-1}(k)}}\frac{e^{-ikx}}{V}\sqrt{\frac{\pi V}{\beta\tilde{G}^{-1}(k)}}e^{\sum_k\frac{\beta\tilde{J}^2_{im}(k)}{V\tilde{G}^{-1}(k)}} \quad . \tag{A.12}$$

Transforming back to real space, the partition function becomes

$$Z_J = \frac{2\sqrt{2}}{V}\prod_{k=-\infty}^{\infty}\sqrt{\frac{\pi V\tilde{G}(k)}{\beta}}e^{\frac{\beta}{2}\int dxdyJ(x)G(x-y)J(y)} \quad . \tag{A.13}$$

Using the expansion of Green's function in Fourier's space,

$$G(x-y) = \frac{1}{V}\sum_k \tilde{G}(k)e^{-ik(x-y)} = \sum_k \lambda_k \phi_k(x-y) \quad , \tag{A.14}$$

one finds that its determinant corresponds to the product of its eigenvalues, i.e.

$$\det\left[\frac{G(x-y)}{\beta}\right] = \prod_k \frac{\lambda_k}{\beta} = \prod_k \frac{\tilde{G}(k)}{\beta} \quad . \tag{A.15}$$

Thus, the partition function takes the final form

$$Z_J = \sqrt{\det\left[\frac{G(x-y)}{\beta}\right]}\, e^{\frac{\beta}{2}\int dxdy J(x)G(x-y)J(y)} \quad . \tag{A.16}$$

This finally yields the Hubbard-Stratonovich transformation

$$\int D\phi e^{\frac{\beta}{2}\int dxdy\phi(x)G^{-1}(x-y)\phi(y)+\beta\int dxJ(x)\phi(x)} = \sqrt{\det\left[\frac{G(x-y)}{\beta}\right]}\, e^{\frac{\beta}{2}\int dxdy J(x)G(x-y)J(y)} \quad . \tag{A.17}$$

Appendix B

The Coulombic Potential

Here, we solve the electrostatic Green's equation (4.6)
$(\nabla_r \epsilon(\mathbf{r}))\,(\nabla_r v_c(\mathbf{r},\mathbf{r}')) = -\frac{e^2}{k_B T}\delta(\mathbf{r}-\mathbf{r}')$
in a three dimensional bulk electrolyte where $\epsilon(\mathbf{r}) = \epsilon_m$ and $v_c(\mathbf{r},\mathbf{r}') = v_c(\mathbf{r}-\mathbf{r}')$. Imposing the two conditions above originating from the translational symmetry in the bulk liquid, Eq.(4.6) becomes

$$\nabla^2_{\mathbf{r}} v_c(\mathbf{r}-\mathbf{r}') = -\frac{e^2}{\epsilon_w k_B T}\delta(\mathbf{r}-\mathbf{r}') = -4\pi l_B \delta(\mathbf{r}-\mathbf{r}') \quad . \tag{B.1}$$

Transforming both sides of the equation into Fourier space, one obtains

$$\tilde{v}_c(k) = \frac{4\pi l_B}{k^2} \quad . \tag{B.2}$$

Substituting Eq.(B.2) in the Fourier transform of $v_c(\mathbf{r}-\mathbf{r}')$, i.e.

$$v_c(\mathbf{r}-\mathbf{r}') = \int \frac{d^3k}{(2\pi)^3} e^{-ik|\mathbf{r}-\mathbf{r}'|}\tilde{v}_c(k) \quad , \tag{B.3}$$

carrying out the Fourier integral, one finally obtains the Coulomb Green's function

$$v_c(\mathbf{r}-\mathbf{r}') = \frac{l_B}{|\mathbf{r}-\mathbf{r}'|} \quad . \tag{B.4}$$

Appendix C

Electrostatic Green's Function in Slit Geometry

Here, we derive the electrostatic Green's function for the slit geometry in Fig.(5.1). In order to derive the Green's equation, we consider first the DH kernel in Eq.(4.25), i.e.

$$v_{DH}^{-1}(\mathbf{r},\mathbf{r}') = -\frac{1}{\beta e^2}\overrightarrow{\nabla}.\epsilon(\mathbf{r})\overrightarrow{\nabla}.\delta(\mathbf{r}-\mathbf{r}') + 2n_b z^2\delta(\mathbf{r}-\mathbf{r}') \quad , \tag{C.1}$$

where n_b is the bulk ion concentration, and z the ion valency. Next, we note that the DH kernel satisfies the convolution relation

$$\int d\mathbf{r}'' v_{DH}^{-}1(\mathbf{r},\mathbf{r}'')v_{DH}(\mathbf{r}'',\mathbf{r}') = \delta(\mathbf{r}-\mathbf{r}') \quad . \tag{C.2}$$

Due to translational symmetry in the x-y plane, the DH Green's function satisfies the identity $v_{DH}(\mathbf{r},\mathbf{r}') = v_{DH}(\mathbf{r}_{||}-\mathbf{r}'_{||},z,z')$. Exploiting this symmetry, the Green's function can be Fourier expanded as

$$v_{DH}(\mathbf{r},\mathbf{r}') = \int \frac{d^2\mathbf{k}}{(2\pi)^2} e^{i\mathbf{k}(\mathbf{r}_{||}-\mathbf{r}'_{||})}\tilde{v}_{DH}(k,z,z') \quad . \tag{C.3}$$

Combining Eqs.(C.1)-(C.3), the Fourier-transformed Green's equation follows as

$$[\epsilon(z)\delta_z^2 - \epsilon(z)k^2 - \epsilon_w\kappa^2]\tilde{v}_{DH}(k,z,z') = -4\pi l_B\epsilon_w \quad . \tag{C.4}$$

Solving Eq.(C.4), one obtains the DH Green's function in the piecewise form

$$\tilde{v}_{DH}(z \leq 0, z' \leq 0) = \tilde{v}_b(z - z') + \frac{2\pi l_B}{p} \frac{\Delta(1 - e^{-2kd})}{1 - \Delta^2 e^{-2kd}} e^{p(z+z')} \quad , \tag{C.5}$$

$$\tilde{v}_{DH}(z \geq d, z' \geq d) = \tilde{v}_b(z - z') + \frac{2\pi l_B}{p} \frac{\Delta(1 - e^{-2kd})}{1 - \Delta^2 e^{-2kd}} e^{p(2d-z-z')} \quad , \tag{C.6}$$

$$\tilde{v}_{DH}(z \leq 0, z' \leq 0) = \tilde{v}_b(z - z') + \frac{2\pi l_B}{p} \frac{(1 - \Delta^2)e^{(p-k)d} + \Delta^2 e^{-2kd} - 1}{1 - \Delta^2 e^{-2kd}} e^{-p|z-z'|} \quad , \tag{C.7}$$

for $z' \leq 0$ and $z \geq d$ or $z' \geq d$ and $z \leq 0$.
Here, we defined the dielectric discontinuity function

$$\Delta = \frac{\epsilon_w p - \epsilon_m k}{\epsilon_w p + \epsilon_m k} \quad , \tag{C.8}$$

and the screening function

$$p = \sqrt{\kappa^2 + k^2} \quad , \tag{C.9}$$

with the Fourier transform of the bulk Green's function

$$\tilde{v}_b(z - z') = \frac{2\pi l_B}{p} e^{-p|z-z'|} \quad . \tag{C.10}$$

Appendix D

Code

The plots have been generated with Mathematica 11.3.0.0,
Licence number: 4944-3239.